Title

Distribution and morphology of calcitonin gene-related peptide (CGRP) innervation in flat mounts of whole rat atria and ventricles.

Permalink

https://escholarship.org/uc/item/7dr7f53n

Authors

Chen, Jin
Bendowski, Kohlton
Bizanti, Ariege
et al.

Publication Date

2024-02-01

DOI

10.1016/j.autneu.2023.103127

Peer reviewed

Distribution and Morphology of Calcitonin Gene-Related Peptide (CGRP) Innervation in Flat Mounts of Whole Rat Atria and Ventricles

Jin Chen[#,1], **Kohlton T. Bendowski**[#,1], **Ariege Bizanti**[1], **Yuanyuan Zhang**[1], **Jichao Ma**[1], **Donald B. Hoover**[2], **David Gozal**[3], **Kalyanam Shivkumar**[4], **Zixi (Jack) Cheng**[1]

[1]Burnett School of Biomedical Sciences, College of Medicine, University of Central Florida, Orlando, FL 32816.

[2]Department of Biomedical Sciences, James H. Quillen College of Medicine, East Tennessee State University, Johnson City, TN 37614.

[3]Office of the Dean, Joan C. Edwards School of Medicine, Marshall University, Huntington, WV 25701.

[4]Department of Medicine, Cardiac Arrhythmia Center and Neurocardiology Research Program of Excellence, University of California, Los Angeles, CA 90095

Abstract

Calcitonin gene-related peptide (CGRP) is widely used as a marker for nociceptive afferent axons. However, the distribution of CGRP-IR axons has not been fully determined in the whole rat heart. Immunohistochemically labeled flat-mounts of the right and left atria and ventricles, and the interventricular septum in rats for CGRP were assessed with a Zeiss imager to generate complete montages of the entire atria, ventricles, and septum, and a confocal microscope was used to acquire detailed images of selected regions. We found that 1) CGRP-IR axons extensively innervated all regions of the atrial walls and the walls of the great vessels including the sinoatrial node region, auricles, atrioventricular node region, superior/inferior vena cava, left pre-caval vein, and pulmonary veins. 2) CGRP-IR axons formed varicose terminals around individual neurons in some cardiac ganglia but passed through other ganglia without making appositions with cardiac

Corresponding authors: Jin Chen (jin.chen@ucf.edu). Burnett School of Biomedical Sciences, College of Medicine, University of Central Florida, 4110 Libra Blvd., Orlando, FL 32816, USA. Fax: +1 4078230956, Zixi (Jack) Cheng (zixi.cheng@ucf.edu). Burnett School of Biomedical Sciences, College of Medicine, University of Central Florida, 4110 Libra Blvd., Orlando, FL 32816, USA. Fax: +1 4078230956.
[#] =These authors contributed equally to the study.

neurons. 3) Varicose CGRP-IR axons innervated the walls of blood vessels. 4) CGRP-IR axons extensively innervated the right/left ventricular walls and interventricular septum. Our data shows the rather ubiquitous distribution of CGRP-IR axons in the whole rat heart at single-cell/axon/ varicosity resolution for the first time. This study lays the foundation for future studies to quantify the differences in CGRP-IR axon innervation between sexes, disease models, and species.

Keywords

Calcitonin gene-related peptide; heart; vasculature; intrinsic cardiac ganglia; atria; ventricles

Introduction

Calcitonin gene-related peptide-immunoreactive (CGRP-IR) axons innervate the heart and are involved in sensory and motor cardiac functions. These functions include nociception, vasodilation, sinoatrial (SA) node function, regulation of atrial muscle contractility, and inflammation [1–10]. Some studies show that CGRP may possess chronotropic properties as well [11–13]. Previously, we characterized the distribution and morphology of CGRP-IR and substance P-immunoreactive (SP-IR) axons in flat-mounts (or equally "whole mounts" as we used in the previous paper) of the whole right and left atria of mice [14], as well as the distribution and morphology of catecholaminergic axons within the right and left atria and ventricles of C57BL6/J mice [15,16]. However, the distribution and morphology of CGRP-IR axons in the whole heart (atria, ventricles, and interventricular septum) of rats has not been extensively characterized.

CGRP-IR axons innervate multiple targets in the heart including the sinoatrial (SA) node, atrioventricular (AV) node, conducting tissue, and blood vessels (particularly the large arteries and pulmonary veins) [9,17–21]. CGRP-IR axons have been found within the intrinsic cardiac ganglia (ICG) and the interconnective nerve bundles between the ICG, but have not been shown to form pericellular or basket endings around individual ICG principal neurons such as those that are typically found in vagal efferent innervation [22–28]. The atria typically contain a greater abundance of CGRP-IR axons, however many of these axons are also found in the ventricles, particularly in the middle region [29,30]. A greater amount of CGRP-IR axons has been consistently reported in the right ventricle compared to the left ventricle in several species [17,29].

The thickness of the cardiac muscle poses a difficult challenge for immunofluorescence studies due to the large amount of background autofluorescence and heterogeneous antibody penetration. Because of this, most studies use thin tissue sectioning. Nevertheless, using thin sectioning techniques to illustrate CGRP-IR axon distribution disrupts the natural continuity of the axons and does not allow for visualization of their complete structure [9,17,18,20]. In previous studies, CGRP-IR axons were shown using partial flat-mounts, but the images only included small segments of the axons and their distribution in the entire heart was not analyzed [19,25,28,29,31]. In addition, flat-mount tissues were sometimes cut to focus on specific targets like ganglia and blood vessels, but this does not show the full continuity of

the structures [27]. As a result, the distribution of CGRP-IR axons in the entire heart has yet to be fully characterized.

In this study, we aimed to show the distribution of CGRP-IR axons in all regions of the heart by preparing whole rat hearts as flat mounts of the left and right atria, ventricles, and interventricular septum. We used CGRP immunohistochemistry and imaging via a conventional fluorescence microscope (Zeiss M2 Imager) and a confocal microscope. High resolution images were captured of the entirety of each tissue and assembled into complete photo montages. In addition, we acquired higher magnification images showing the fine details of the axons and their distribution around crucial cardiac targets including the cardiac muscle, ICG neurons, and blood vessels, such that for the first time the distribution of CGRP-IR axons in the whole organ flat-mount of the rat heart at the single-cell/axon/ varicosity scale is revealed. This work lays the methodological foundation for future studies aimed at further characterization and quantification of the differences in the distribution and morphology of CGRP-IR axons between species, sexes, and disease models.

Materials and Methods

Animals and ethical statement.

All procedures were performed as approved by the University of Central Florida (UCF) Institutional Animal Care and Use Committee (HURON PROTO202000115) and strictly followed the guidelines established by the National Institutes of Health NIH and the ARRIVE 2.0 guidelines. Healthy male Sprague-Dawley rats (RRID: RGD_737903; Envigo RMS, LLC, Indianapolis, IN) (n=6; 2–3 months; weighing: 200–350 g) were used and housed together in cages (n=2 per cage) with sawdust bedding (changed 3 times per week) in a room with controlled environmental conditions such as humidity and temperature. Rats were kept on a 12:12 light:dark cycle (6:00 AM to 6:00 PM) and were provided food and water *ad libitum*. Efforts were made to minimize the number of animals used and minimize discomfort.

Whole heart dissection and flat-mount preparation.

Rats were first deeply anesthetized with isoflurane (5%; 5–10 minutes), with an oxygen flow rate of 1 liter per minute. When the animals were not responsive to the hind-toe pinch withdrawal reflex, the chest was opened and an injection of heparin (100 units) was made in the apex of the left ventricle. After the inferior vena cava was cut to drain the blood and perfusate, a needle was inserted into the left ventricle and the perfusion began. The rats were first perfused with 500 ml of 37–40 °C phosphate-buffered saline (0.1 M PBS, pH = 7.4) followed by 300 ml paraformaldehyde (4%; 4 °C). The tissues were separated in the same manner that is shown in Figure 1 of Bizanti et al., 2023[15]. The heart, lungs, and trachea were removed immediately after perfusion and stored in 4 % paraformaldehyde for at least 24 hours at 4 °C. The atria and ventricles were separated at the atrial-ventricular groove, and the left and right atria and ventricles were separated. The left atrium was prepared with the entrance portions of all pulmonary veins (PVs) attached and the right atrium was prepared with the superior vena cava (SVC), inferior vena cava (IVC) and left precaval vein (LPCV) attached [32].

Immunohistochemistry.

Dissected tissues were washed 3 times for 15 min in 0.01 M PBS (pH = 7.4) in a 6-well plate on an orbital shaker to remove the remaining fixative. To prevent non-specific binding and enhance antibody penetration, the atria were fully submerged in a blocking solution (2% bovine serum albumin, 10% normal donkey serum, 2% Triton X-100, 0.08% NaN3 (in 0.1 M PBS, pH = 7.4)) for 5 days (atria) at 4 ºC. Anti-CGRP primary antibody (Cell Signaling, Danvers, MA; Cat # 14959, RRID: AB_2798662; 1:200) was mixed with the primary solution (2% bovine serum albumin, 4% normal donkey serum, 0.5% Triton X-100, 0.08% NaN3 in 0.1 M PBS, pH = 7.4) and incubated with the tissues for 5 days (for atria) or 7 days (for ventricles) at 4 ºC. Tissues were thoroughly washed 6 times for 10 min in PBST (phosphate buffered saline with Triton X-100; 0.5% Triton X-100 in 0.01 M PBS) to remove unbound primary antibodies. Tissues were then kept in the dark and incubated in a fluorescent secondary antibody solution (Alexa Fluor 488; Thermo Fisher, Waltham, MA, Cat# A21202, RRID:AB_141607; 1:100) overnight at room temperature. Unbound secondary antibodies were removed by washing 6 times for 10 minutes in PBS at room temperature. Rat ventricles were pretreated with methanol and the immunolabeling procedures outlined in [33] to obtain better penetration for thicker tissue. In these steps PBST was substituted for PtwH (solution of PBS, Tween, and Heparin; not used in this study) and the immunolabeling concentrations were substituted for the values given above; **note:** the clearing step was omitted entirely. Tissues were then mounted onto glass slides and flattened with lead weights for either 2 days (20 lbs for atria) or 3 weeks (30 lbs for ventricles) at 4 ºC. Slides were dehydrated in four ascending concentrations of ethanol (75%, 95%, 100%, and 100%) for 2 min in each concentration, followed by 2×10 min washes in 100% xylene. Coverslips were then attached using DEPEX mounting medium (Electron Microscopy Sciences #13514) and allowed to dry overnight. Negative controls, which excluded primary antibodies, showed no immunoreactivity, confirming that nonspecific binding of secondary antibodies did not occur. Antibody specificity was tested by Cell Signaling Technology using Western Blot and immunofluorescence (https://www.cellsignal.com/products/primary-antibodies/cgrp-d5r8f-rabbitmab/14959). Western Blot analysis shows a single band at the correct molecular weight of CGRP in TT cells but not in HeLa cells. Moreover, confocal immunofluorescent analysis of TT and HeLa cells confirms that CGRP were in TT cells but not in HeLa cells. Thus, we believe the CGRP antibodies used in this study are specific.

Image acquisition.

Hundreds of overlapping maximum projection images from stacks of optical sections (z-step: 1.5 μm for atria and 2 μm for the ventricles) from each tissue were captured using a Zeiss M2 Imager (20x lens; NA 0.8) and stitched back together seamlessly to yield full photo montages of the right and left atria and ventricles. An LED light source with a 488 nm wavelength was used to visualize the CGRP-IR axons in the tissues. A Leica TCS SP5 laser-scanning confocal microscope (40x oil immersion lens; NA 1.25; z-step: 1 μm) was used to capture detailed images of CGRP-IR axons and their targets in selected locations of the heart. An argon–krypton laser (488 nm) was used to visualize CGRP-IR axons in the tissue, and a helium-neon laser (543 nm) was used to detect the autofluorescence of the tissues in the background (e.g., cardiac muscles, ganglionic cells, and blood vessels).

Modifications, including brightness and contrast adjustments, and scale bar additions, were performed using Photoshop or FIJI ImageJ software [34]. Of the 6 rat hearts that were used in this study, we showed the representative cases from each tissue in our figures (RA, LA, RV, LV, and IVS).

Results

Distribution and morphology of CGRP-IR axons and terminals in the right and left atria flat mounts.

Multiple bundles containing CGRP-IR axons entered the right atrium along the superior vena cava (SVC; or equally the right cranial vein) and/or in between the SVC and the left pre-caval vein (LPCV; or equally the left cranial vein). These bundles split into smaller branches and formed a complex network of axons that also innervated all areas of the tissue (Figures 1 and 3). Several CGRP-IR axons were observed within the walls of the LPCV (Figure 3A&B), inferior vena cava (IVC; or equally the caudal vein) (Figure 3E), SVC (Figure 3F), right auricle (Figure 3G), and mid-atrial regions (Figure 3H). CGRP-IR axons also innervated an intrinsic cardiac ganglion (ICG) near the SVC (Figure 3C) and a few ICG near the junction between the LPCV and the RA (or equally the left cranial vein sinus) (Figure 3D). In addition, CGRP-IR axons supplied the sinoatrial (SA) and atrioventricular (AV) node regions (these are the regions of the right atrium close to the SA and AV nodes, respectively) (Figure 4). In this study we use the terms SVC, IVC, and LPCV in place of the terms right cranial vein (RCV), left cranial vein (LCV), and caudal vein (CV), respectively as described by Batulevicius et al., 2003[35]. We use this terminology to avoid confusion between this work and our previous studies[14–16,32]. Moreover, this terminology is also used by established investigators in the field to describe anatomical features in quadrupedal animals[27,36,37].

Large CGRP-IR nerve bundles entered the right atrium along the LPCV, and these bifurcated into smaller individual axons that innervated the area of the right atrial wall near the interatrial septum (Figures 1 and 3A). This bundle would then split off into smaller branches that further ramified into individual axons, which innervated the tissue of the LPCV. However, it is important to note that the axons, which originated from these bundles, also innervated the LA in addition to the RA.

CGRP-IR axons entered the LA as large bundles along the middle atrium before bifurcating into smaller branches and individual axons, which innervated most of the left atrial wall(Figure 2). Multiple large CGRP-IR axon bundles entered the LA and bifurcated into smaller bundles, which ramified into individual axons that innervated the large ICG within the SA node plexus near the interatrial septum [32] (Figure 5A). Two medium-sized ganglia (Figure 5B and C) and one additional large sized ganglion (Figure 5D) were innervated with CGRP-IR axons. A CGRP-IR bundle was found within the wall of the auricle and ramified into many varicose endings that innervated the cardiac muscle of the auricle (Figure 5E). All of the pulmonary veins were also innervated with a dense network of CGRP-IR axons (Figure 5F–H).

To determine whether or not CGRP-IR axons innervated different locations and tissue layers in the atria, we used a Leica TCS SP5 laser scanning confocal microscope to acquire detailed images of distinct locations within each atria. A 488 nm ArKr laser was used to excite the fluorescent secondary antibody bound to the CGRP and a 594 nm HeNe laser was used to excite the autofluorescence of the cardiac tissue. CGRP-IR axons densely innervated the auricle wall of the right and left atria. Complex axonal networks were observed in the center of the auricle and extended outward to the edge of the auricle as well (Figures 6&7 A and B). Furthermore, a dense network of CGRP-IR axons was found within the middle region of both the left and right atria (Figures 6&7 C). Dense CGRP-IR networks were also observed in the SA and AV node regions (Figure 4). Using single-optical section images of the deeper muscular layers of these same areas, it was shown that a dense network of CGRP-IR axon terminals innervate the myocardial muscle layers of each of these regions (Figures 4A' and B'; 6&7 A', B', and C'). Large bifurcating CGRP-IR axon bundles were very common in the epicardial layer of the atria (Figure 8A). These bundles split into fine terminal endings that projected into the myocardial layer where they formed a complex network within the cardiac muscle (Figure 8B).

CGRP-IR axons wrap around individual ICG neurons and pass through other ICG.

Several intrinsic cardiac ganglia (ICG) were observed on the epicardium of the atria (Figures 1, 2, 3C&D, 5B–D, and 9). Many of these ICG were observed in the LA between the left auricle and the junction of the PVs with the LA (or equally the pulmonary sinuses) particularly near the SA and AV nodes regions of the RA (Figures 2 and 5A). On the LA, a network of CGRP-IR axons can be observed in the middle of the atrium connecting the ICG. One medium-sized ICG was observed within the RA near the junction of the SVC with the RA (or equally the right cranial vein sinus) (Figure 3C) and 3 medium-sized ganglia were observed at the junction between the LPCV and the RA (Figure 3D). Dense networks of CGRP-IR axons were observed within all ICG (Figure 9 A–H). Some CGRP-IR axon networks within the ICG formed varicose endings, which made several appositions with the principal neurons of the ICG (Figure 9C). On the other hand, some bundles of CGRP-IR axons traveled through the ICG without making varicose appositions with individual principal neurons (Figure 9 E and F). In other cases, ICG showed both patterns, with some axons wrapping around and forming tight appositions and others seeming to pass through the ganglion (Figure 9 G and H). None of the ICG neurons observed in this study were CGRP-IR.

CGRP-IR axons innervate blood vessels.

CGRP-IR axons and axon bundles were observed within the walls of the great vessels (SVC, IVC, LPCV, and PVs) of the RA and LA (Figures 1–3; 5). In addition, CGRP-IR axons were found to tightly surround arterioles. While these blood vessels are difficult to see in the maximum projection images, they were clearly visible within the optical sections. CGRP-IR axons ran in parallel with these blood vessels and formed varicose endings which tightly wrapped around the perimeter of the vessels. A montage of multiple maximum projection images shows a branching arteriole along the outside of the IVC (red arrows in Figure 10A). Confocal maximum projection and single optical section images showed that CGRP-IR axons made varicose appositions with this arteriole (Figure 10B &10B').

CGRP-IR axons extensively innervate the right and left ventricles, and interventricular septum.

Leica confocal and Zeiss M2 Imager microscopy revealed an extensive distribution of CGRP-IR axons within the walls of the right and left ventricles and the interventricular septum. CGRP-IR axons entered the ventricular wall as large bundles through the base of the heart before bifurcating into smaller branches that ramified in the direction of the apex and formed fine terminal endings throughout the tissue (Figures 11 and 13). A similar distribution of CGRP-IR axons was observed in the interventricular septum (Figure 16).

A dense network of CGRP-IR axons was observed in the base, middle and apex of the left and right ventricular free walls, and the interventricular septum (Figures 12, 14, and 16). Single optical section images taken in the myocardial region of each location showed that CGRP-IR axon terminals innervated the myocardial muscle layer, however, in contrast to the epicardium, the myocardium contained only single axons rather than bundles (Figure 15). To compare the innervation pattern of the ventral and dorsal sides of the ventricles and interventricular septum, maximum projection confocal images were taken of each side of each tissue. For the right ventricle, the ventral and dorsal sides consisted of large CGRP-IR axon bundles which bifurcated into single axons. For the left ventricle, the pattern was similar between the ventral and dorsal sides in which large bifurcating CGRP-IR axon bundles gave rise to smaller bundles and ultimately individual CGRP-IR axons.

Discussion

In the present study, we have described the distribution and morphology of CGRP-IR axons within all cardiac regions. This work is highly novel as it is the first to show this distribution using flat-mount preparations of the entire organ regions of the rat heart (atria and ventricles). Our earlier work showed the distribution of CGRP-IR axons in flat-mounts of the *mouse* atria[14], but the work presented here expanded our technique to label these axons in the much thicker *rat* heart including the ventricles. This was a very difficult feat and, to our knowledge, has not been done in other studies. Moreover, understanding the innervation of the rat heart, particularly the ventricles, is very informative towards studies which use physiological heart failure models[38]. Previous studies relied on sectioned tissues to study this distribution, however our use of whole organ flat-mount tissue preparations allowed us to preserve the continuity of the axons within the organ and thus enhance the accuracy of such projections. Some studies used flat-mount tissue to show CGRP-IR axons in the heart, however only small areas were shown which does not allow for the analysis of the larger pattern within the entire heart.

Within the atria, we've shown that CGRP-IR axons entered the heart as large axon bundles along the great vessels (SVC, LPCV, and the junction between the PVs and the LA) before ramifying into smaller branches and individual axons which supplied the majority of the cardiac tissue. *Within the RA,* large axon bundles entered mainly along the LPCV. A single large axon was frequently observed along the LPCV, which would split into 2–4 smaller branches and innervate all regions of the tissue including the LPCV, ICG, AV node region, and the auricle. Additional large axon bundles entered through the SVC which innervated the SA and AV nodes, the auricle, and mid-atrium region. *Within the LA,* large axon bundles

entered near the junction between the PVs and the LA. These axons would then bifurcate many times eventually forming individual axons which innervated all areas of the tissue including the ICG, blood vessels, mid-atrial region, and the auricle. *Within the ventricles and interventricular septum,* CGRP-IR axons entered as large axon bundles through the base before bifurcating multiple times towards the apex and covering the majority of the tissue with a network of axons and their terminals. These axons innervated the blood vessels and the epicardial and the myocardial layers.

Distribution of CGRP-IR axons in the right and left atria, ventricles, and interventricular septum.

In a previous study, we showed the distribution and morphology of CGRP-IR axons in the whole organ flat-mount of the right and left atria in mice [14]. Other studies have shown CGRP-IR innervation in selected locations of partial flat-mounts or cryosections of the heart, but such approaches disrupt the continuity of the axons and do not give a complete picture of their distribution. To address this problem, we used a technique developed in our previous studies that uses a combination of whole organ flat-mount preparation and IHC to show the uninterrupted distribution of CGRP-IR axons in the rat atria for the first time [14–16]. In contrast to these previous studies, the current study used rat tissue which is much thicker than mouse tissue. Our method preserved the 3D continuity of these axons without the need for sectioning. Furthermore, neither autofluorescence nor tissue thickness proved to be obstacles for clear image acquisition.

CGRP increases the chronotropic and inotropic activity of the atria [13,39]. Therefore, CGRP is an important neuropeptide in the regulation of the cardiac pacemaker (SA and AV node) and cardiac muscle activity. In our study, CGRP-IR axons were distributed throughout the entirety of both atria which strongly supports these findings. Though CGRP-IR axon innervation was observed in all locations, some locations displayed differing patterns of innervation. For example, large axon bundles were mostly observed in the epicardium of both atria, particularly around the great vessels and middle atrium region, and complex networks of individual axons were observed deeper in the myocardial layers that appear to be analogous in structure to the intramuscular endings found within the colonic structures of mice [40,41]. This suggests that CGRP-IR axons may have different levels of sensation or control depending on the layer/location within the atria.

Our method also allowed us to visualize a complex network of CGRP-IR axons in the RV, LV, and IVS. Similar to the atria, the large axon bundles were most often observed in the epicardium of the ventricles, and a complex network of individual axons was observed in the deeper myocardial layers. The presence of this complex network of axons in both ventricles and the IVS suggests a possible role for CGRP in the regulation of cardiac muscle contractility [6,7,42]. Overall, these results lay the foundation for future studies which will quantify and compare the innervation patterns of different locations within all tissues of the heart. connectome.

CGRP-IR axon innervation of the ICG plexus.

In addition to its extrinsic afferent and efferent innervation, the heart also contains an intrinsic ("little brain") network of neurons which regulate cardiac functions. The cell bodies for these neurons are located within the ICG of the heart. As in our previous study, our results showed several ICG located on the epicardium of both atria, particularly the left atrium [32,43]. Furthermore, our methods preserved the anatomy of these ganglia, which allowed us to fully analyze their structures. Many CGRP-IR axons were found within the ICG which is consistent with other flat-mount studies [14,27]. While many studies like these have found CGRP-IR axons within the ICG, it is unclear whether these nerves have any influence on principal neurons in the ganglia. Physiological studies should explore this in the future.

Within some ganglia, CGRP-IR axons were observed encircling individual principal neurons with varicose endings suggesting that these axons may have made synaptic contacts with ICG neurons, but future studies using techniques like electron microscopy will be needed to confirm this. However, in some cases, CGRP-IR axons would pass through the ganglia as large bundles without making appositions. Some ganglia contained both axons which passed through the ganglia and axons which encircled and formed varicose appositions with principal neurons. The variety of innervation patterns in the ICG suggests that, if CGRP does have some effect on ICG neurons, then CGRP-IR axons may have differing control levels depending on the ganglion which they innervate. This observation is consistent with previous studies that reported heterogeneous functional responses from distinct cardiac ganglia. For example, electrical stimulation of the ganglion near the SA node in the rat heart elicited a negative chronotropic effect, whereas stimulation of the ganglion near the AV node produced a negative dromotropic effect instead [37].

While several CGRP-IR axons were observed within ICG, no CGRP-IR ICG principal neurons were detected. Furthermore, CGRP-IR axons projecting to the heart and stomach mostly originate from afferent neurons in the dorsal root ganglia (DRG) and do not colocalize with TH or VAChT, and therefore are likely not from efferent origin [44–46]. This suggests that CGRP-IR axons in the heart most likely originate from extrinsic sources rather than being intrinsic.

CGRP-IR axon innervation of the blood vessels.

CGRP is one of the most potent vasodilators that has ever been documented [10,47–50]. Using our method of flat-mount tissue preparation, we were able to preserve the structure of the blood vessels within the atria. Blood vessels were identified using a combination of tissue structure observations for branching patterns consistent with typical blood vessel structure, and analyzing single optical sections to identify hollow spaces in the tissue. We observed several CGRP-IR axons wrapping around the length of blood vessels, which is consistent with the role of CGRP as a vasodilating neuropeptide [9,17]. Moreover, dense networks of CGRP-IR axons were found in the great vessels of the heart (SVC, IVC, LPCV, and PVs) which were also the entry points for the large CGRP-IR axon bundles. CGRP application triggered relaxation in the pulmonary arteries and veins, and calcitonin receptor-like receptors have been observed in the tissue of the pulmonary artery implying a

possible role for CGRP in regulation of pulmonary blood flow and filling of the left atrium [51,52].

Clinical and functional implications.

CGRP is a neuropeptide involved in the transmission of pain originating from both the somatic and visceral organs [53]. Stimulation of nociceptive nerves by capsaicin, ischemia, low-pH, and bradykinin leads to a release of CGRP in the spinal cord as well as a local release in the cardiac tissue [54–56]. Thus, CGRP-IR nerves serve a dual sensory-efferent function termed an "axon reflex" [57]. Local release of CGRP as a result of myocardial ischemia has a potent vasodilating effect on the coronary arteries which increases blood flow to the heart tissue [54,58]. Along with other neuropeptides such as substance P, CGRP is a key factor in the cardioprotective benefits of ischemic pre- and post-conditioning in myocardial infarction [1]. Due to their crucial role in the regulation of cardiac functions, CGRP-IR axons are an important target for the treatment of cardiovascular diseases. Deletion of TRPV1 led to an increase in cardiac hypertrophy and inflammation following transverse aortic constriction through local release of CGRP [59]. Denervation of spinal afferent axons improved heart conditions by attenuating the cardiac sympathetic efferent reflex in chronic heart failure rats. In the initial phases of heart failure the activation of spinal afferent activity will trigger an increase in sympathetic drive to the heart which is beneficial at first because it restores much needed blood flow to the body. However, over the long-term this increased sympathetic activity will be detrimental to cardiac function [38]. Treatments are being developed to manipulate sympathetic axons that are showing signs of success [60]. However, the main targets for these types of treatments include the spinal DRG and the vagal nodose ganglia (VNG) which project to different organs and systems. Because of this, stimulation of these targets to treat diseases may lead to many off-target effects that can be dangerous for the patients. To avoid this, we must have a better understanding of the topographical distribution of nociceptive axons within the target organs such as the heart. By identifying specific populations of axons and associating them with their parent nerves we will gain a better understanding of where these therapies should be applied to deliver safe and precise treatments for cardiovascular diseases.

Previously we studied the pathological remodeling of vagal efferent nerves in cardiovascular diseases [61–64]. Now, we are able to apply these methods to the study of the alterations within CGRP-IR nerves in the context of cardiovascular disease. Considering the fact that diabetes and aging result in degeneration of sensory axons, this may lead to an increase in damage from myocardial ischemia since the protective mechanisms of CGRP-IR axons may not be activated [1,4,50]. In one of our recent studies, we mapped the catecholaminergic innervation of the atria and ventricles in mice exposed to chronic intermittent hypoxia (CIH; a model for sleep apnea) to determine the morphological remodeling (Cheng et al, 2023 unpublished data). In the future, we may use this same technique to determine the morphological changes of spinal afferent nerves in diseases, such as diabetes, CIH, and aging. Furthermore, whether or not the increase in CIH-induced sympathetic drive to the heart is in part a result of loss of spinal afferent innervation has yet to be confirmed [38]. Many studies have shown that cardiovascular diseases can alter autonomic reflexes in the heart. Whether this change is due to remodeling of nociceptive axons at the level of the

heart has not yet been explored. However, the work we present here will serve as a baseline comparative resource.

Limitations of the study.

The method used in this study allowed for the visualization of the distribution of CGRP-IR axons in the whole organ flat-mount of the rat heart, an approach that overcame the limitations of other techniques such as cryosectioning, and therefore produced images that captured the uninterrupted morphology of afferent axons in these tissues. Though this work is highly novel and will provide the basis for many other studies in the future, there are some limitations to this study that should be addressed. While the 2D morphology of CGRP-IR axons in the tissues was preserved, the flattening of the tissue caused the 3D position of the axons to become distorted, and therefore the exact depth of the axons within the tissue could not be determined. However, the tissue layers were still able to be differentiated, and enabled to accurately determine which axons were in the epicardium and which axons were in the myocardium. Moreover, it would have been preferable to have connected atria samples, an impossibility prescribed by the intrinsic and unavoidable thickness of the tissue.

Summary.

Our study expanded our understanding of the sensory innervation of the heart and will serve as the foundation for future studies of sex and species differences, as well as studies focused on pathological remodeling in the context of cardiovascular diseases. In the future, the techniques described in this study will be used to perform quantitative analysis to determine the extent that the density of CGRP-IR axons differs between regions and tissue layers of the heart. These axons will be traced and digitized and integrated into a virtual 3D scaffold of the heart. Furthermore, we will explore the potential morphological remodeling of spinal afferent axons in the heart in disease models such as diabetes and CIH.

Acknowledgements

Data Availability Statement

The high-quality figures and data associated with this study are available from the corresponding author upon reasonable request.

References

1. Randhawa PK & Jaggi AS A review on potential involvement of TRPV1 channels in ischemia–reperfusion injury. J. Cardiovasc. Pharmacol. Ther 23, 38–45 (2018). [PubMed: 28466657]
2. Tritthart HA et al. Membrane Actions of Calcitonin Gene-Related Peptide in Cardiac and Smooth Muscle Myocytesa. Ann. N. Y. Acad. Sci 657, 216–227 (1992). [PubMed: 1637086]
3. Al-Rubaiee M. et al. Inotropic and lusitropic effects of calcitonin gene-related peptide in the heart. Am. J. Physiol.-Heart Circ. Physiol 304, H1525–H1537 (2013). [PubMed: 23585136]
4. Kumar A, Potts JD & DiPette DJ Protective Role of α-Calcitonin Gene-Related Peptide in Cardiovascular Diseases. Front Physiol 10, 821 (2019). [PubMed: 31312143]

5. Rubino A, Ralevic V. & Burnstock G. Calcitonin gene-related peptide (CGRP)-evoked inotropism during hyper- and hypo-sensory-motor innervation in rat atria. J. Auton. Pharmacol 17, 121–127 (1997). [PubMed: 9234082]

6. Saetrum Opgaard O, Hasbak P, de Vries R, Saxena PR & Edvinsson L. Positive inotropy mediated via CGRP receptors in isolated human myocardial trabeculae. Eur. J. Pharmacol 397, 373–382 (2000). [PubMed: 10844137]

7. Saetrum Opgaard O, de Vries R, Tom B, Edvinsson L. & Saxena PR Positive inotropy of calcitonin gene-related peptide and amylin on porcine isolated myocardium. Eur. J. Pharmacol 385, 147–154 (1999). [PubMed: 10607870]

8. Sigrist S. et al. Specific receptor and cardiovascular effects of calcitonin gene-related peptide. Endocrinology 119, 381–389 (1986). [PubMed: 3013594]

9. Sugiyama A, Kobayashi M, Tsujimoto G, Motomura S. & Hashimoto K. The First Demonstration of CGRP-lmmunoreactive Fibers in Canine Hearts: Coronary Vasodilator, Inotropic and Chronotropic Effects of CGRP in Canine Isolated, Blood-Perfused Heart Preparations. Jpn. J. Pharmacol 50, 421–427 (1989). [PubMed: 2789300]

10. Benemei S, Nicoletti P, Capone JG & Geppetti P. CGRP receptors in the control of pain and inflammation. Curr. Opin. Pharmacol 9, 9–14 (2009). [PubMed: 19157980]

11. Gennari C. & Fischer JA Cardiovascular action of calcitonin gene-related peptide in humans. Calcif. Tissue Int 37, 581–584 (1985). [PubMed: 3937576]

12. Franco-Cereceda A. et al. Cardiovascular effects of calcitonin gene-related peptides I and II in man. Circ. Res 60, 393–397 (1987). [PubMed: 3495374]

13. Miyauchi T, Ishikawa T, Sugishita Y, Saito A. & Goto K. Effects of capsaicin on nonadrenergic noncholinergic nerves in the guinea pig atria: role of calcitonin gene-related peptide as cardiac neurotransmitter. J. Cardiovasc. Pharmacol 10, 675–682 (1987). [PubMed: 2450238]

14. Li L. et al. Distribution and morphology of calcitonin gene-related peptide and substance P immunoreactive axons in the whole-mount atria of mice. Auton. Neurosci 181, 37–48 (2014). [PubMed: 24433968]

15. Bizanti A. et al. Catecholaminergic axon innervation and morphology in flat-mounts of atria and ventricles of mice. J. Comp. Neurol 531, 596–617 (2023). [PubMed: 36591925]

16. Zhang Y. et al. Topographical mapping of catecholaminergic axon innervation in the flat-mounts of the mouse atria: a quantitative analysis. Sci. Rep 13, 4850 (2023). [PubMed: 37029119]

17. Gerstheimer F. & Metz J. Distribution of calcitonin gene-related peptide-like immunoreactivity in the guinea pig heart. Anat. Embryol. (Berl.) 175, 255–260 (1986). [PubMed: 3548482]

18. Onuoha GN, Kaya Alpar E, Nicholls D. & Buchanan K. Calcitonin gene-related peptide, neuropeptide Y and atrial natriuretic peptide distribution in guinea pig heart from paraffin wax-embedded and formalin-cryoprotected tissues. Histochem. J 31, 617–622 (1999). [PubMed: 10579631]

19. Pauza DH et al. Neuroanatomy of the murine cardiac conduction system: A combined stereomicroscopic and fluorescence immunohistochemical study. Auton. Neurosci 176, 32–47 (2013). [PubMed: 23403121]

20. Uddman R, Edvinsson L, Ekblad E, Håkanson R. & Sundler F. Calcitonin gene-related peptide (CGRP): perivascular distribution and vasodilatory effects. Regul. Pept 15, 1–23 (1986). [PubMed: 3532219]

21. Ursell PC, Ren CL, Albala A. & Danilo P Jr Nonadrenergic noncholinergic innervation. Anatomic distribution of calcitonin gene-related peptide-immunoreactive tissue in the dog heart. Circ. Res 68, 131–140 (1991). [PubMed: 1984857]

22. Cheng Z, Powley TL, Schwaber JS & Doyle III FJ Projections of the dorsal motor nucleus of the vagus to cardiac ganglia of rat atria: an anterograde tracing study. J. Comp. Neurol 410, 320–341 (1999). [PubMed: 10414536]

23. Cheng Z. & Powley TL Nucleus ambiguus projections to cardiac ganglia of rat atria: an anterograde tracing study. J. Comp. Neurol 424, 588–606 (2000). [PubMed: 10931483]

24. Cheng Z. Vagal cardiac efferent innervation in F344 rats: Effects of chronic intermittent hypoxia. Auton. Neurosci 203, 9–16 (2017). [PubMed: 27839717]

25. Forsgren S, Moravec M. & Moravec J. Catecholamine-synthesizing enzymes and neuropeptides in rat heart epicardial ganglia; an immunohistochemical study. Histochem. J 22, 667–676 (1990). [PubMed: 1706694]

26. Moravec M, Moravec J. & Forsgren S. Catecholaminergic and peptidergic nerve components of intramural ganglia in the rat heart. An immunohistochemical study. Cell Tissue Res. 262, 315–327 (1990). [PubMed: 1706221]

27. Richardson R, Grkovic I. & Anderson C. Immunohistochemical analysis of intracardiac ganglia of the rat heart. Cell Tissue Res. 314, 337–350 (2003). [PubMed: 14523644]

28. Rysevaite K. et al. Immunohistochemical characterization of the intrinsic cardiac neural plexus in whole-mount mouse heart preparations. Heart Rhythm 8, 731–738 (2011). [PubMed: 21232628]

29. Pauziene N. et al. Innervation of the rabbit cardiac ventricles. J. Anat 228, 26–46 (2016). [PubMed: 26510903]

30. Pauziene N. et al. Neuroanatomy of the Pig Cardiac Ventricles. A Stereomicroscopic, Confocal and Electron Microscope Study. Anat. Rec 300, 1756–1780 (2017).

31. Pauza DH et al. A combined acetylcholinesterase and immunohistochemical method for precise anatomical analysis of intrinsic cardiac neural structures. Ann. Anat. - Anat. Anz 196, 430–440 (2014).

32. Ai J. et al. Morphology and topography of nucleus ambiguus projections to cardiac ganglia in rats and mice. Neuroscience 149, 845–860 (2007). [PubMed: 17942236]

33. Goodyer WR et al. Transcriptomic Profiling of the Developing Cardiac Conduction System at Single-Cell Resolution. Circ. Res 125, 379–397 (2019). [PubMed: 31284824]

34. Collins TJ ImageJ for microscopy. BioTechniques 43, S25–S30 (2007).

35. Batulevicius D, Pauziene N. & Pauza DH Topographic morphology and age-related analysis of the neuronal number of the rat intracardiac nerve plexus. Ann. Anat. - Anat. Anz 185, 449–459 (2003).

36. Paton JFR et al. Advancing respiratory–cardiovascular physiology with the working heart–brainstem preparation over 25 years. J. Physiol 600, 2049–2075 (2022). [PubMed: 35294064]

37. Sampaio KN, Mauad H, Spyer KM & Ford TW Differential chronotropic and dromotropic responses to focal stimulation of cardiac vagal ganglia in the rat. Exp. Physiol 88, 315–327 (2003). [PubMed: 12719756]

38. Wang H-J, Wang W, Cornish KG, Rozanski GJ & Zucker IH Cardiac Sympathetic Afferent Denervation Attenuates Cardiac Remodeling and Improves Cardiovascular Dysfunction in Rats With Heart Failure. Hypertension 64, 745–755 (2014). [PubMed: 24980663]

39. Ishikawa T, Okamura N, Saito A. & Goto K. Effects of calcitonin gene-related peptide (CGRP) and isoproterenolon the contractility and adenylate cyclase activity in the rat heart. J. Mol. Cell. Cardiol 19, 723–727 (1987). [PubMed: 2826795]

40. Spencer NJ, Kyloh M. & Duffield M. Identification of different types of spinal afferent nerve endings that encode noxious and innocuous stimuli in the large intestine using a novel anterograde tracing technique. PloS One 9, e112466 (2014).

41. Spencer NJ, Kyloh MA, Travis L. & Dodds KN Identification of spinal afferent nerve endings in the colonic mucosa and submucosa that communicate directly with the spinal cord: The gut-brain axis. J. Comp. Neurol 528, 1742–1753 (2020). [PubMed: 31909835]

42. Schlier A. et al. CGRP-α responsiveness of adult rat ventricular cardiomyocytes from normotensive and spontaneously hypertensive rats. Eur. J. Cell Biol 88, 227–241 (2009). [PubMed: 19128857]

43. Achanta S. et al. A Comprehensive Integrated Anatomical and Molecular Atlas of Rat Intrinsic Cardiac Nervous System. iScience 23, 101140 (2020).

44. Hoover DB, Shepherd AV, Southerland EM, Armour JA & Ardell JL Neurochemical diversity of afferent neurons that transduce sensory signals from dog ventricular myocardium. Auton. Neurosci 141, 38–45 (2008). [PubMed: 18558516]

45. Ma J. et al. Topographical organization and morphology of substance P (SP)-immunoreactive axons in the whole stomach of mice. J. Comp. Neurol 531, 188–216 (2023). [PubMed: 36385363]

46. Spencer NJ, Zagorodnyuk V, Brookes SJ & Hibberd T. Spinal afferent nerve endings in visceral organs: recent advances. Am. J. Physiol.-Gastrointest. Liver Physiol 311, G1056–G1063 (2016). [PubMed: 27856418]

47. Sohn I, Sheykhzade M, Edvinsson L. & Sams A. The effects of CGRP in vascular tissueclassical vasodilation, shadowed effects and systemic dilemmas. Eur. J. Pharmacol 881, 173205 (2020).

48. Kee Z, Kodji X. & Brain SD The Role of Calcitonin Gene Related Peptide (CGRP) in Neurogenic Vasodilation and Its Cardioprotective Effects. Front. Physiol 9, 1249 (2018). [PubMed: 30283343]

49. Argunhan F. & Brain SD The Vascular-Dependent and -Independent Actions of Calcitonin Gene-Related Peptide in Cardiovascular Disease. Front. Physiol 13, (2022).

50. Russell FA, King R, Smillie S-J, Kodji X. & Brain SD Calcitonin Gene-Related Peptide: Physiology and Pathophysiology. Physiol. Rev 94, 1099–1142 (2014). [PubMed: 25287861]

51. Coupe M, Mak J, Yacoub M, Oldershaw P. & Barnes P. Autoradiographic mapping of calcitonin gene-related peptide receptors in human and guinea pig hearts. Circulation 81, 741–747 (1990). [PubMed: 2155072]

52. McCormack DG, Salonen RO & Barnes PJ Effect of sensory neuropeptides on canine bronchial and pulmonary vessels in vitro. Life Sci. 45, 2405–2412 (1989). [PubMed: 2481796]

53. Urits I. et al. An evidence-based review of CGRP mechanisms in the propagation of chronic visceral pain. Best Pract. Res. Clin. Anaesthesiol 34, 507–516 (2020). [PubMed: 33004162]

54. Franco-Cereceda A, Saria A. & Lundberg JM Differential release of calcitonin gene-related peptide and neuropeptide Y from the isolated heart by capsaicin, ischaemia, nicotine, bradykinin and ouabain. Acta Physiol. Scand 135, 173–187 (1989). [PubMed: 2784250]

55. Lundberg JM, Franco-Cereceda A, Alving K, Delay-Goyet P. & Lou Y-P Release of Calcitonin Gene—Related Peptide from Sensory Neuronsa. Ann. N. Y. Acad. Sci 657, 187–193 (1992). [PubMed: 1637084]

56. Wang X. & Fiscus RR Lactic acid potentiates bradykinin- and low-pH-induced release of CGRP from rat spinal cord slices. Am. J. Physiol.-Endocrinol. Metab 273, E92–E98 (1997).

57. Maggi CA Tachykinins and calcitonin gene-related peptide (CGRP) as co-transmitters released from peripheral endings of sensory nerves. Prog. Neurobiol 45, 1–98 (1995). [PubMed: 7716258]

58. Holman JJ, Craig RK & Marshall I. Human alpha- and beta-CGRP and rat alpha-CGRP are coronary vasodilators in the rat. Peptides 7, 231–235 (1986). [PubMed: 3488543]

59. Zhong B, Rubinstein J, Ma S. & Wang DH Genetic ablation of TRPV1 exacerbates pressure overload-induced cardiac hypertrophy. Biomed. Pharmacother. Biomedecine Pharmacother 99, 261–270 (2018).

60. Sverrisdottir YB et al. Human Dorsal Root Ganglion Stimulation Reduces Sympathetic Outflow and Long-Term Blood Pressure. JACC Basic Transl. Sci 5, 973–985 (2020). [PubMed: 33145461]

61. Chen J, Gu H, Wurster RD & Cheng ZJ The protective role of SOD1 overexpression in central mediation of bradycardia following chronic intermittent hypoxia in mice. Am. J. Physiol.-Regul. Integr. Comp. Physiol 320, R317–R330 (2021). [PubMed: 33296277]

62. Gu H. et al. Selective impairment of central mediation of baroreflex in anesthetized young adult Fischer 344 rats after chronic intermittent hypoxia. Am. J. Physiol.-Heart Circ. Physiol 293, H2809–H2818 (2007). [PubMed: 17693540]

63. Lin M. et al. Chronic intermittent hypoxia impairs baroreflex control of heart rate but enhances heart rate responses to vagal efferent stimulation in anesthetized mice. Am. J. Physiol.-Heart Circ. Physiol 293, H997–H1006 (2007). [PubMed: 17384123]

64. Lin M. et al. Structural remodeling of nucleus ambiguus projections to cardiac ganglia following chronic intermittent hypoxia in C57BL/6J mice. J. Comp. Neurol 509, 103–117 (2008). [PubMed: 18425809]

Highlights:

- CGRP-IR axons extensively innervated all regions of the atria including the sinoatrial node region, auricles, atrioventricular node region, superior/inferior vena cava, left pre-caval vein, and pulmonary veins.

- CGRP-IR axons formed varicose terminals around individual neurons in some cardiac ganglia, but passed through other ganglia without making contact with cardiac neurons.

- Varicose CGRP-IR axons innervated blood vessels.

- CGRP-IR axons extensively innervated the right/left ventricles and interventricular septum.
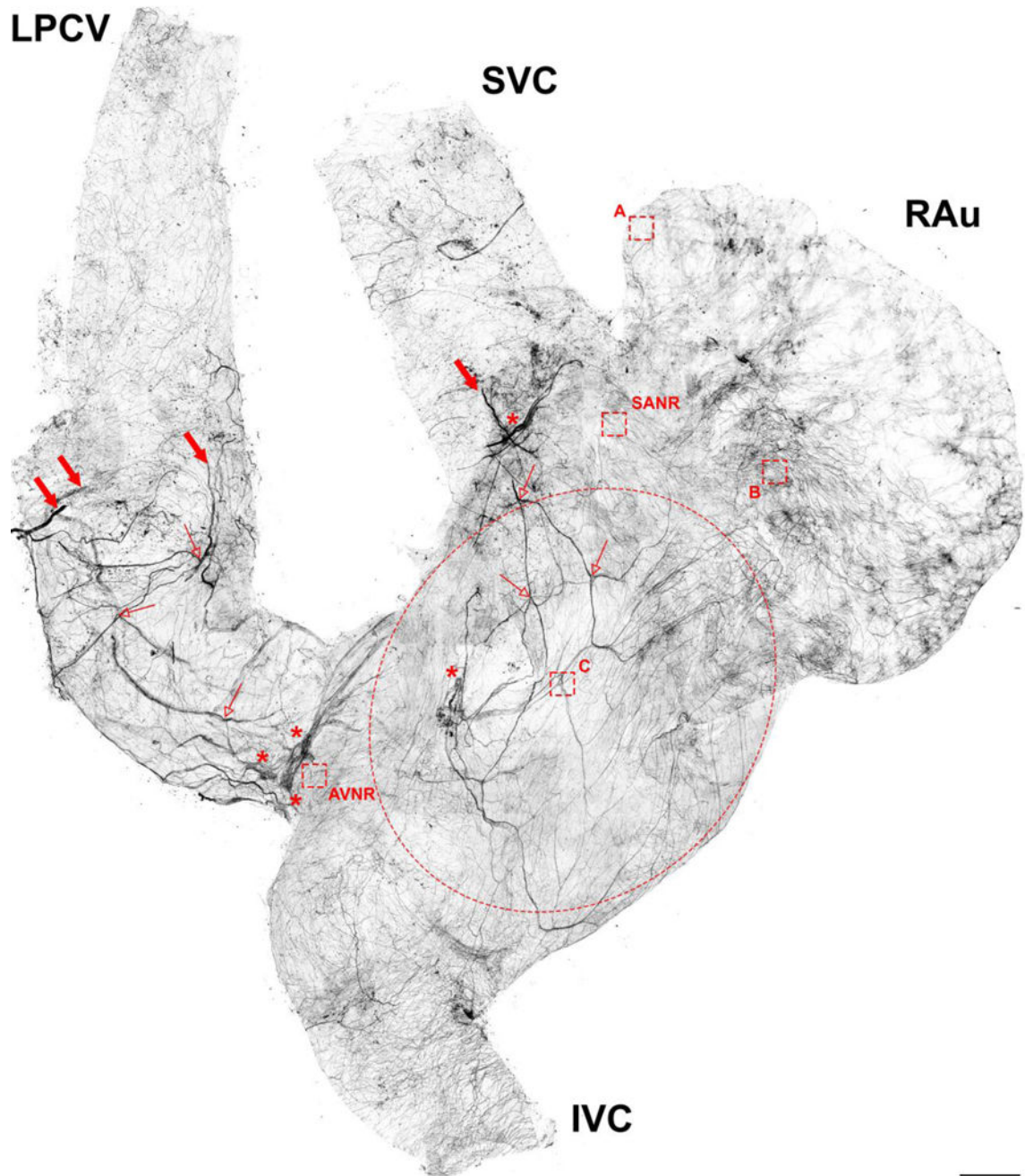
Figure 1.
Distribution of CGRP-IR axons in the rat right atrium (RA). Hundreds of maximum-projection images taken using a Zeiss M2-Imager were stitched together to create a complete montage of the CGRP-IR axon innervation of the rat RA. CGRP-IR axons entered as large bundles near the left pre-caval vein (LPCV) and superior vena cava (SVC) (large arrows) then bifurcated into small bundles (small open arrows) and finally formed single axons and terminals, which distributed throughout the entire tissue. CGRP-IR axons innervated intrinsic cardiac ganglia (asterisks). Boxes A-C correspond to panels A-C in Figure 6. RAu:

right auricle, SVC: superior vena cava, IVC: inferior vena cava, LPCV: left pre-caval vein; SANR: SA node region; AVNR: AV node region; Dotted ellipse: middle-atrium; Scale bar: 1 mm.
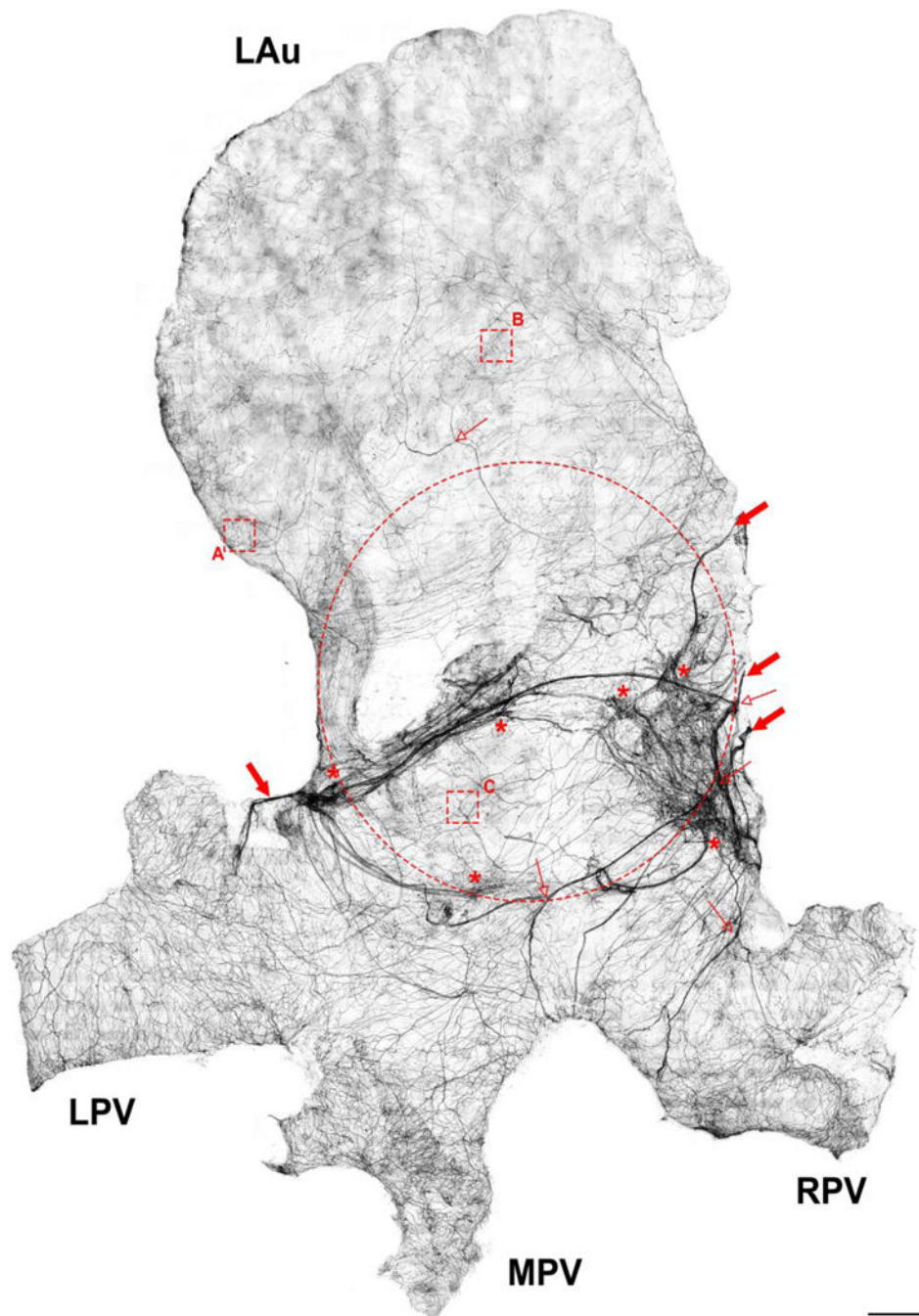
Figure 2.
Distribution of CGRP-IR axons in a rat left atrium. Hundreds of maximum-projection
images taken using a Zeiss M2-Imager were stitched together to create a complete montage
of the CGRP-IR axon innervation of the rat LA. CGRP-IR axons entered as large bundles
(large arrows) then bifurcated into small bundles (small arrows) and finally formed single
axons and terminals, which distributed throughout the entire tissue. CGRP-IR axons
innervated intrinsic cardiac ganglia (asterisks). Boxes A-C correspond to panels A-C in

Figure 7. LAu: left auricle, PV: pulmonary vein; Dotted ellipse: middle-atrium; Scale bar: 1 mm.
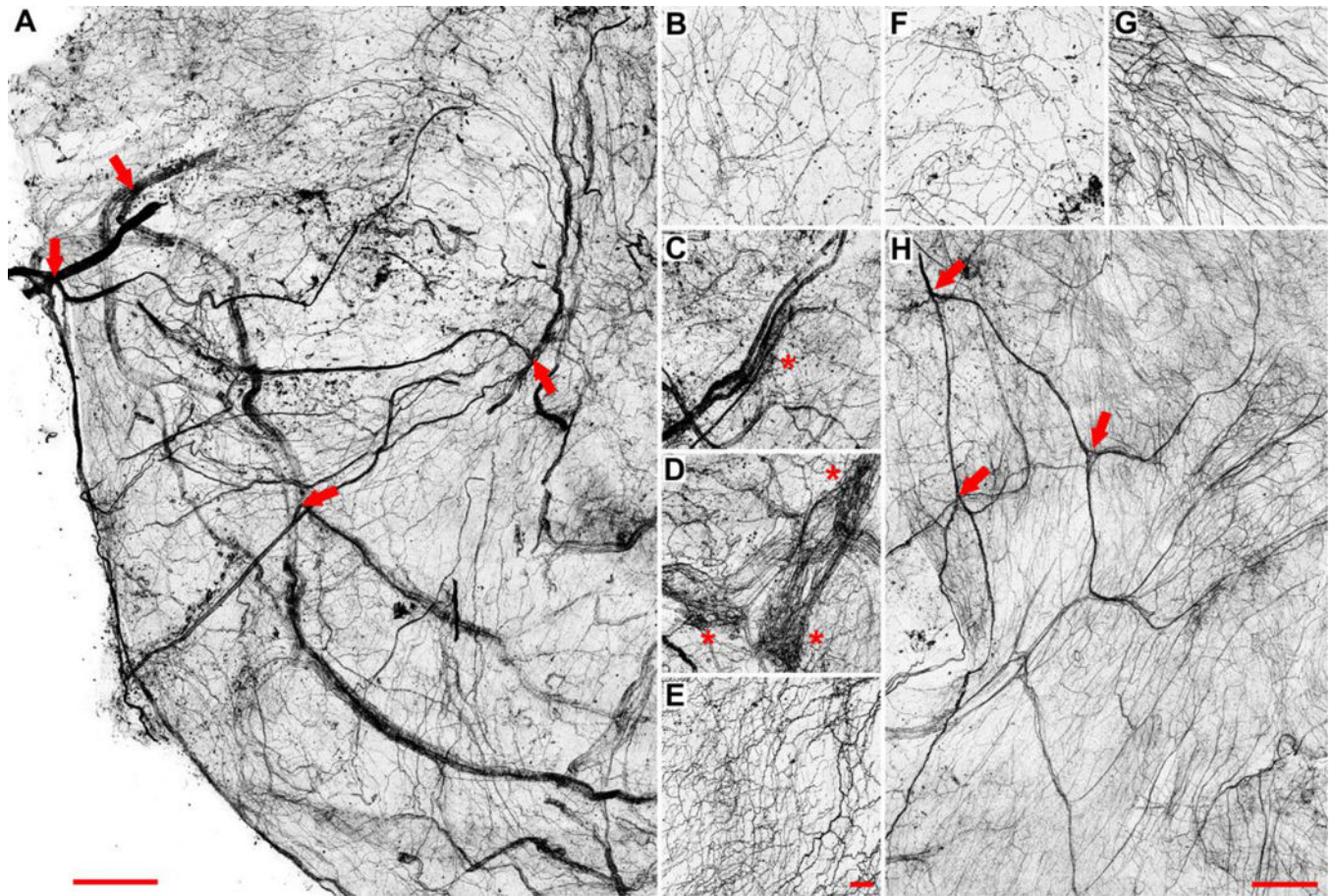
Figure 3.
Zoomed-in views of specific regions of the RA which show the details of CGRP-IR axon
networks. **A:** Large CGRP-IR axon bundles entered along the LPCV and bifurcated into
smaller bundles (arrows) towards the RA. **Note:** though large bundles were found along the
LPCV, it is likely that many of these axons actually innervated the left atrium more than
the right. Many small axon terminals ramified from these axon bundles and innervated the
tissue of the LPCV. **B & E-G:** Various axon terminal networks innervated different regions
of the RA. Dense CGRP-IR axon terminal networks were found in the LPCV (**B**), the IVC
(**E**), the SVC (**F**), and the RAu (**G**). **C:** A medium-sized ICG innervated by a network of
CGRP-IR axons near the SVC (asterisk). **D:** Three medium-sized ICG near the junction of
the LPCV with the RA which were innervated by a network of CGRP-IR axons and formed
dense CGRP-IR interconnectives. **H:** Large CGRP-IR axon bundles entered along the SVC
and bifurcated into smaller axon bundles (arrows). Many of the fine terminal axons in the
RA originated from these axon bundles. Scale bars: **A&H:** 500 μm, **B-G:** 100 μm.

Maximum Projection

Single Optical Section
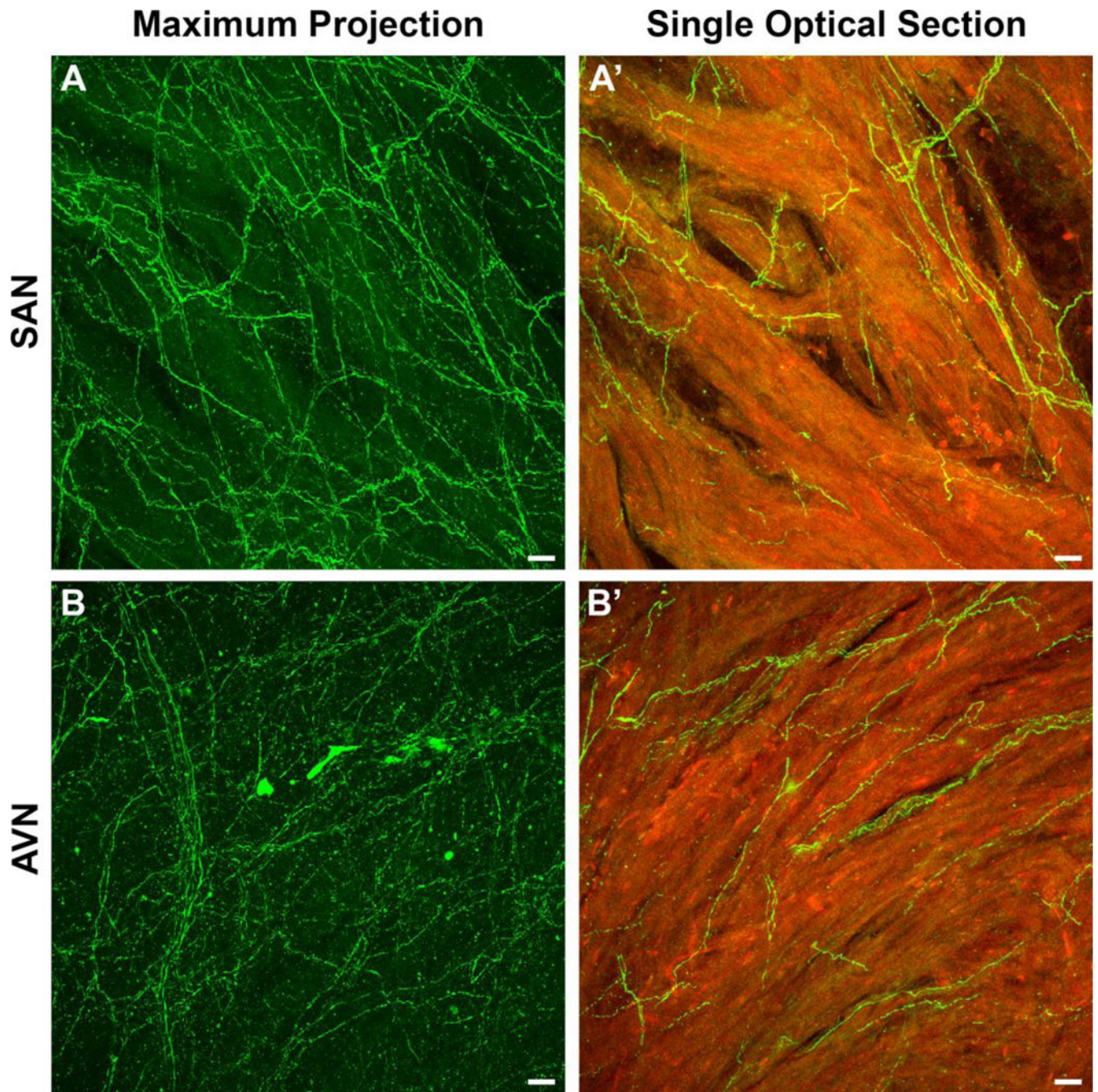
Figure 4.
CGRP-IR innervation of the SA and AV node regions (please zoom into the boxes indicated in the whole montage presented in Figure 1 to see the precise location of each of the panels in this figure). **A:** A maximum projection image showing a dense network of CGRP-IR axons, which was observed in the SA node region of the right atrium. **A':** A single optical section image from **A** showing varicose CGRP-IR axons, which were found within the myocardium. **B:** A maximum projection image showing a dense network of CGRP-IR axons, which was observed in the AV node region of the right atrium. **B':** A single optical

section image from **B** showing varicose CGRP-IR axons which were found within the myocardium. *Green: CGRP-IR; Red: Autofluorescence; Scale bar: 20 μm*
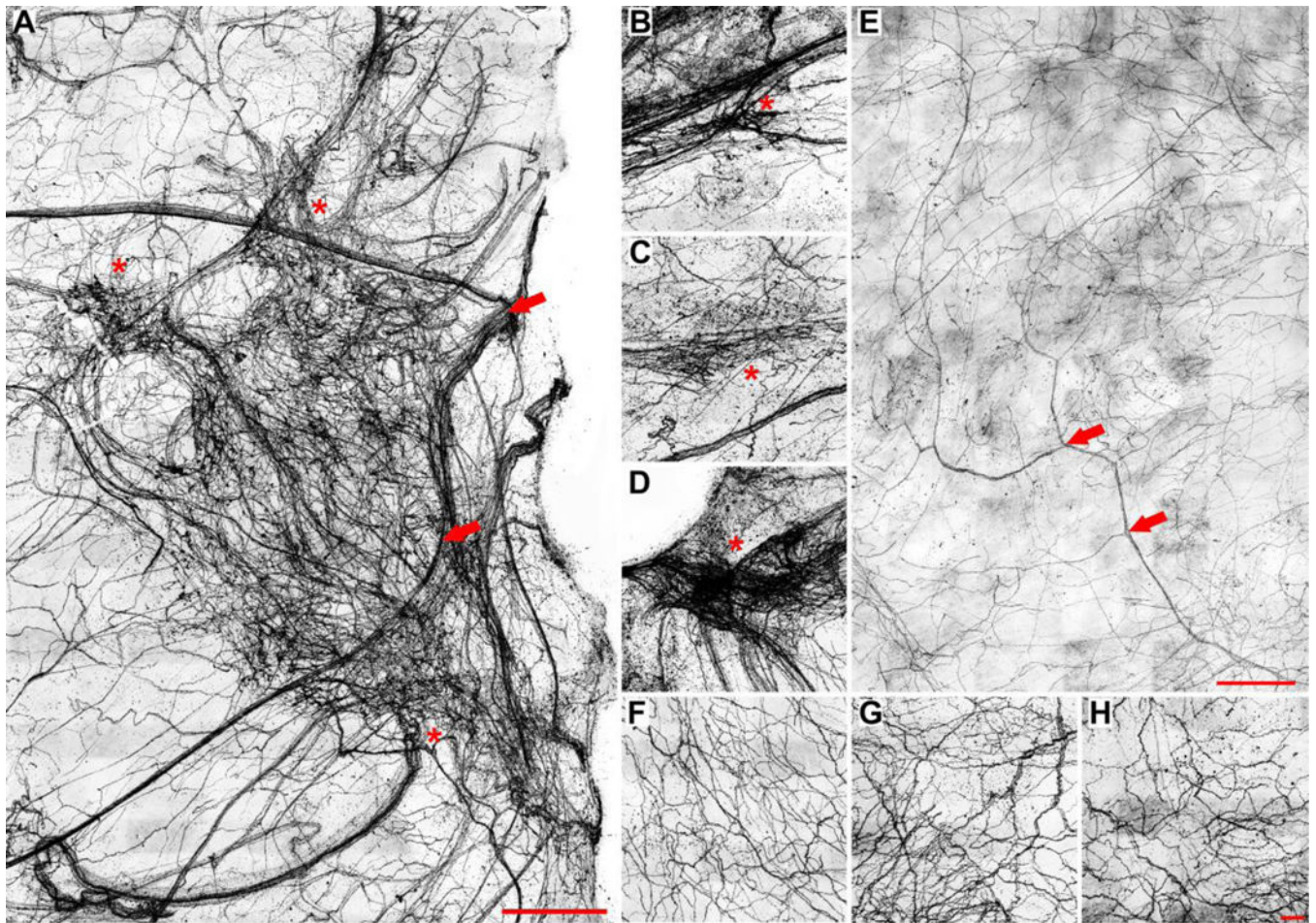
Figure 5.
Zoomed-in views of specific regions of the LA which show the details of CGRP-IR axon networks. **A:** A very dense and complex network of CGRP-IR axons was observed in the SA node ganglionic plexus. Multiple large CGRP-IR axon bundles entered near this area and bifurcated into smaller bundles (arrows). Three large ganglia that were innervated by CGRP-IR axons were observed in this plexus. **B-D:** Two medium size (**B&C**) and one large (**D**) ganglia were innervated by CGRP-IR axons. **E:** A CGRP-IR axon bundle was oriented towards the LAu and bifurcated (arrows) into many small axon terminals which innervated much of the LAu tissue. **F-H:** A dense network of CGRP-IR axons innervated the pulmonary veins. Scale bars: **A&E:** 500 μm, **B-D&F-H:** 100 μm.
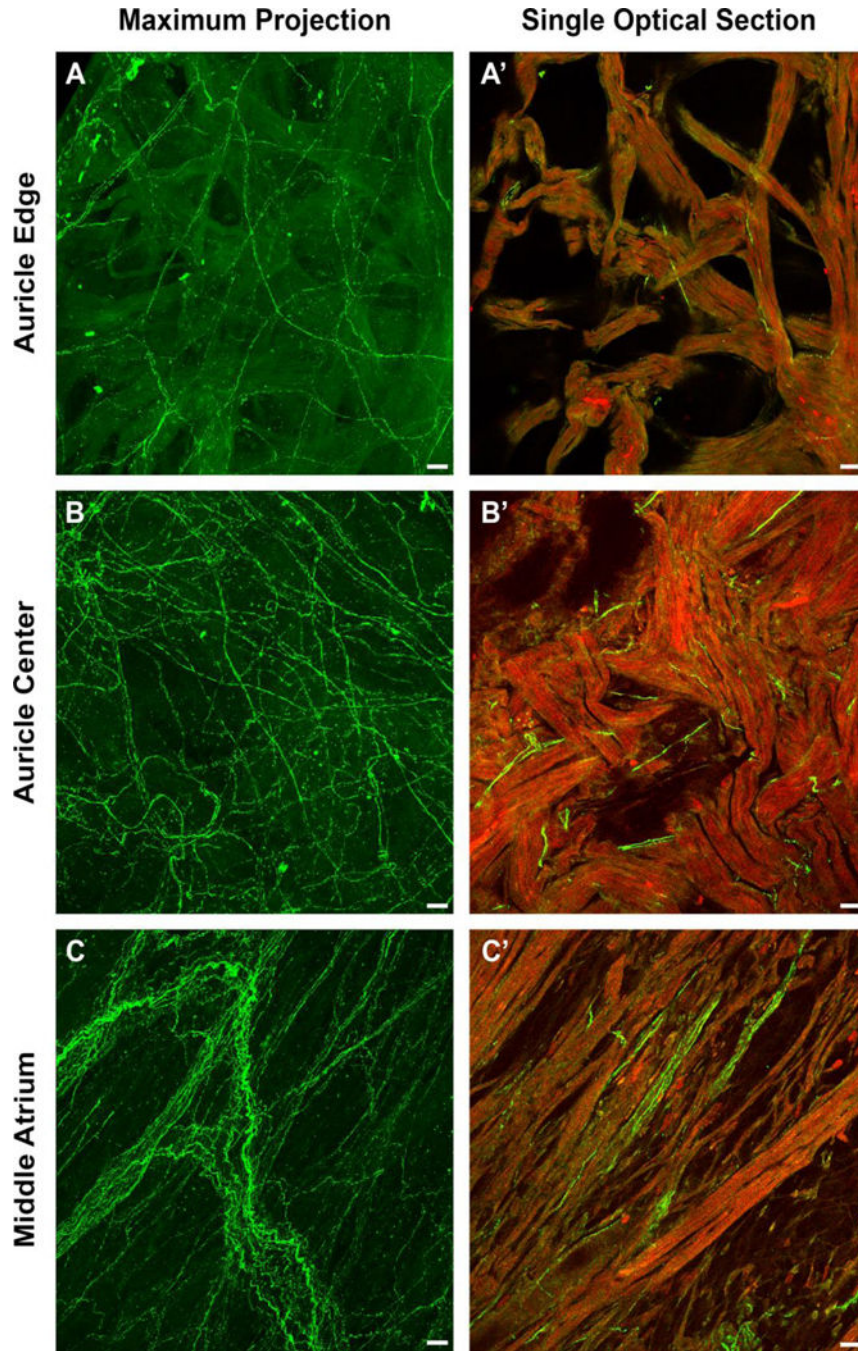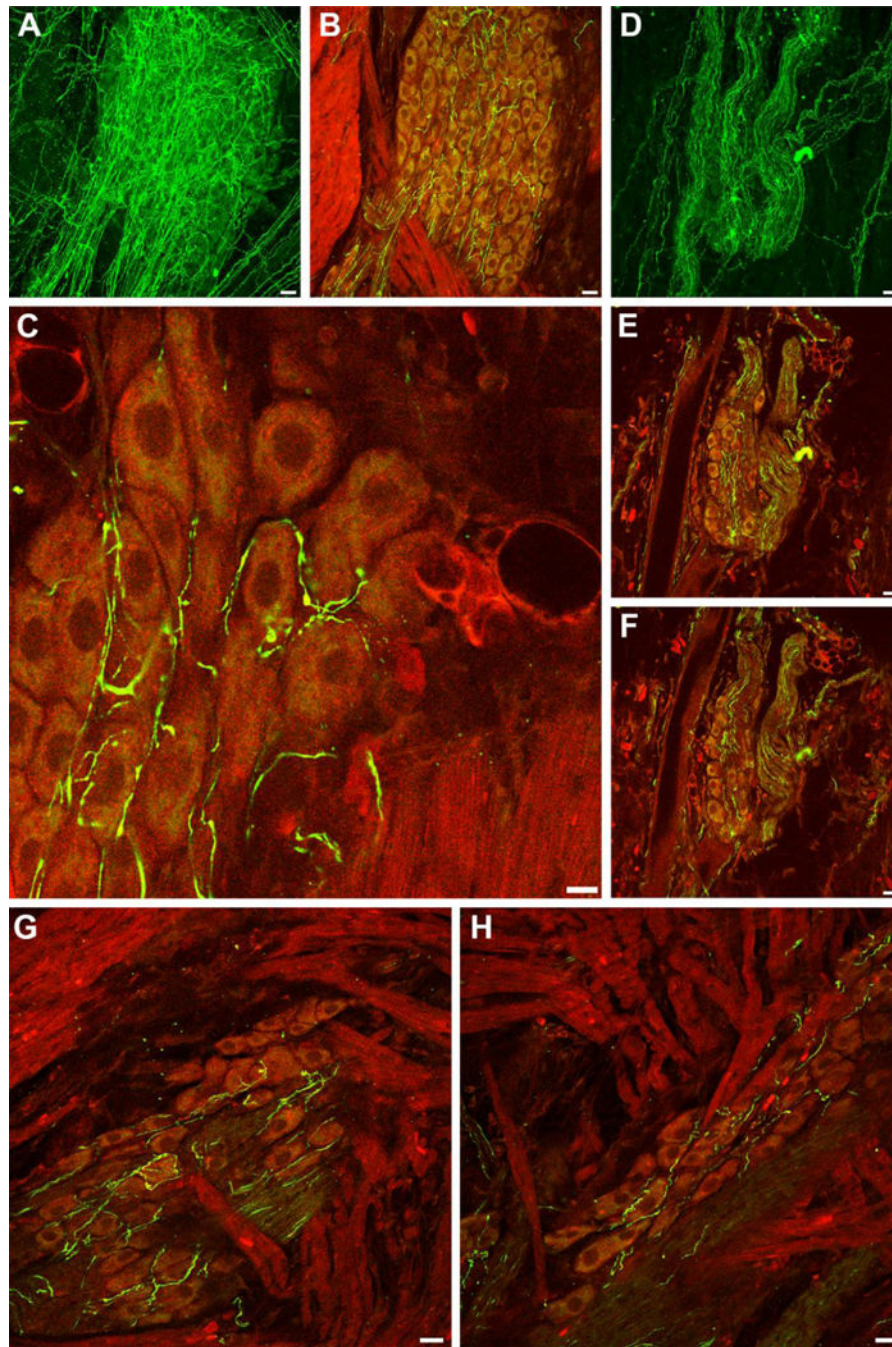
Figure 6.
CGRP-IR axons in the wall of the right atrium (please zoom into the boxes indicated in the whole montage presented in Figure 1 to see the precise location of each of the panels in this figure). CGRP-IR axons innervated all areas of the right atrium. **A-C:** Maximum projection images of the auricle edge, auricle center, and middle atrium, respectively (the boxes indicated in Figure 1) taken with a Leica confocal microscope (40x objective lens; 1 μm z-step). **A'-C':** Single optical section images of A-C. *Green: CGRP-IR; Red: Autofluorescence; Scale bar: 20 μm.*
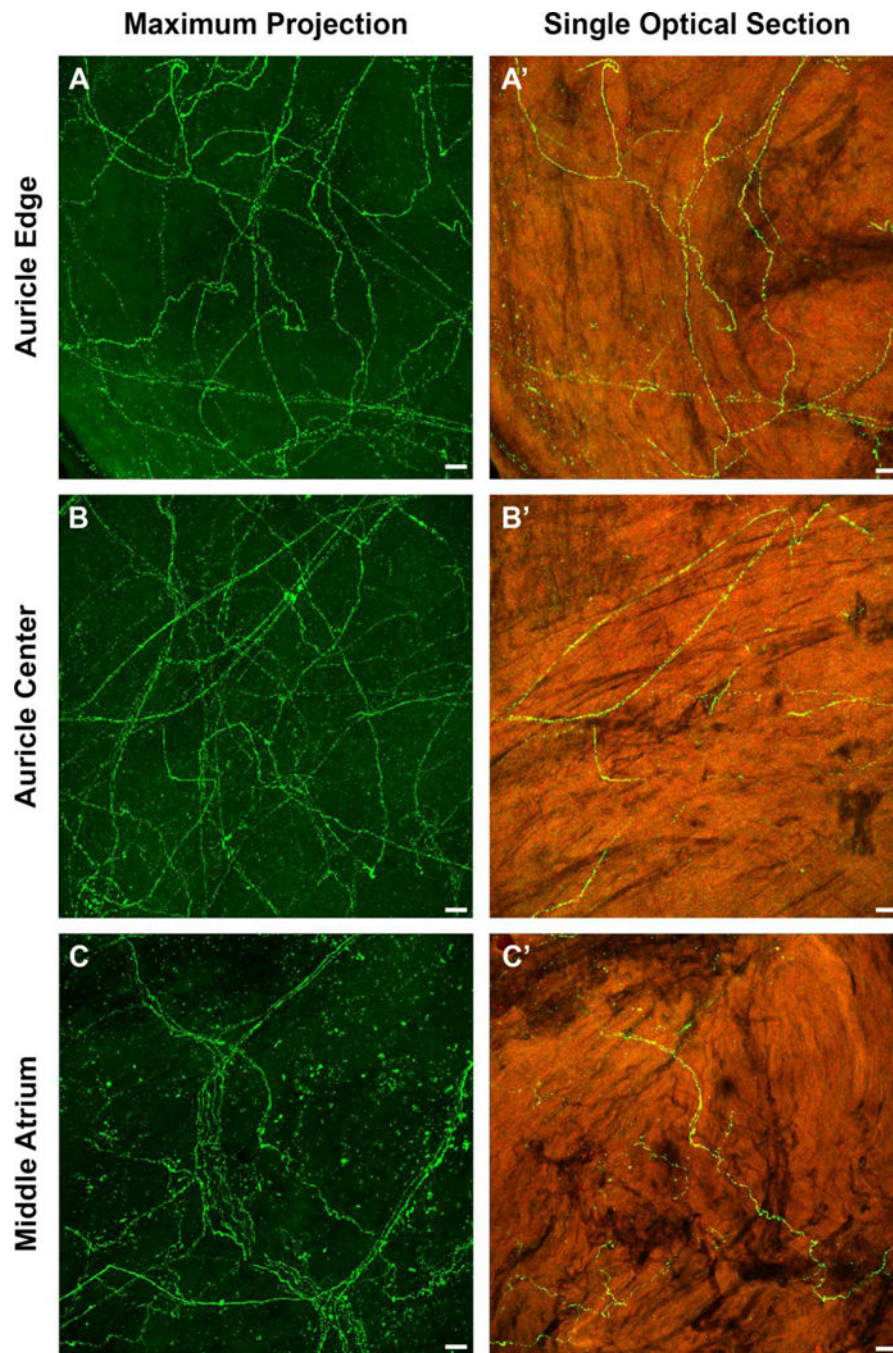
Figure 7.
CGRP-IR axons in the wall of the left atrium (please zoom into the boxes indicated in the whole montage presented in Figure 2 to see the precise location of each of the panels in this figure). CGRP-IR axons innervated all areas of the left atrium. **A-C:** Maximum projection images of the auricle edge, auricle center, and middle atrium, respectively (the boxes indicated in Figure 2) taken with a Leica confocal microscope (40x objective lens; 1 μm z-step). **A'-C':** Single optical section images of A-C. *Green: CGRP-IR; Red: Autofluorescence; Scale bar: 20 μm.*
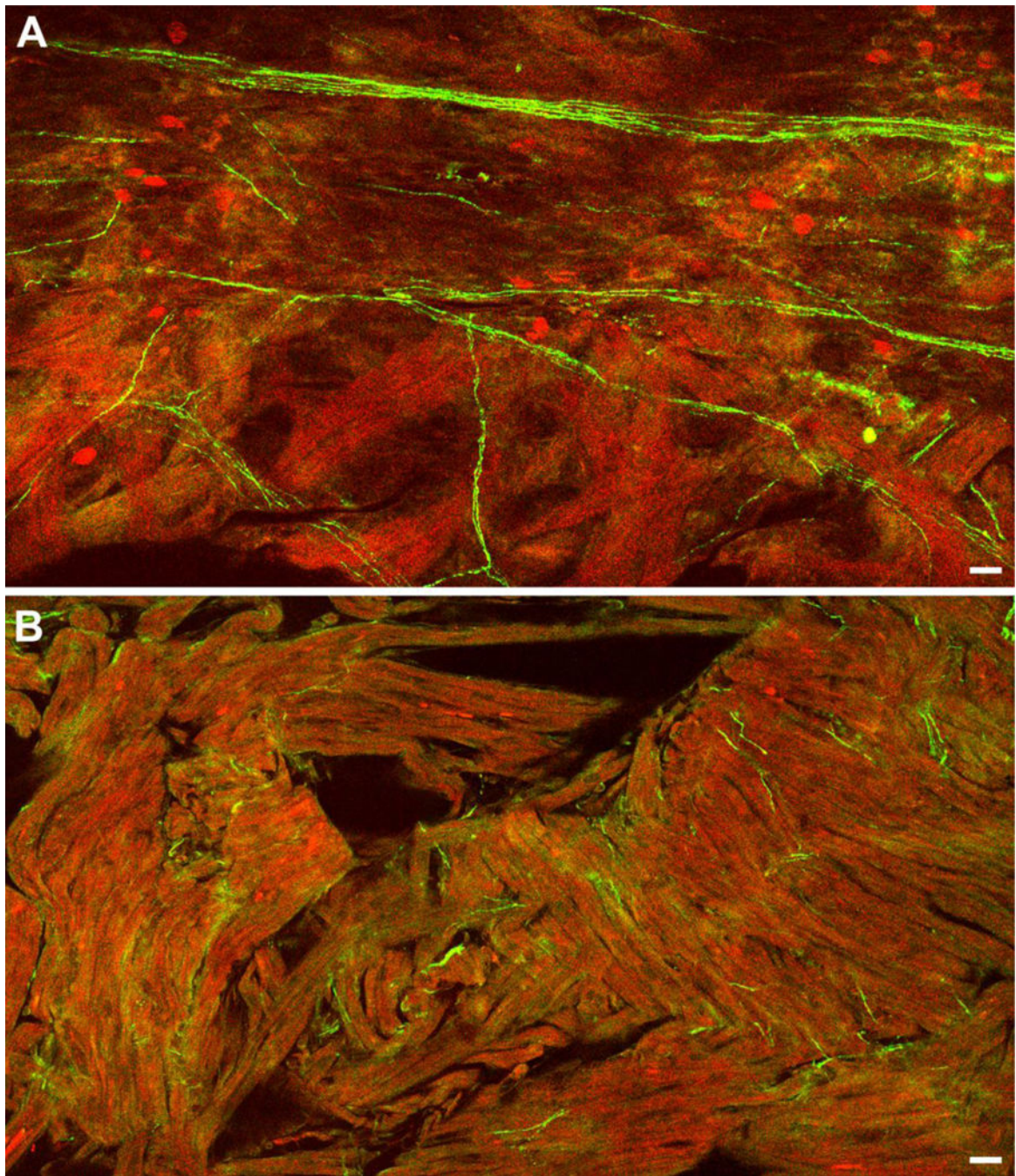
Figure 8.
CGRP-IR axons in the epicardial and myocardial layers of the auricle. **A:** Stitched single optical section images of the epicardial layer near the edge of the right auricle shows that many CGRP-IR axon bundles bifurcated multiple times into individual axons. **B:** Stitched single optical section images of the myocardial layer near the edge of the right auricle in the same location as in **A** that shows a dense network of individual CGRP-IR axons. **Note:** The CGRP-IR axon network in the myocardial layer appears to be much less organized than the epicardial layer. *Green: CGRP-IR; Red: Autofluorescence; Scale bar: 20 μm.*

Figure 9.
CGRP-IR axons innervated intrinsic cardiac ganglia (ICG). **A:** Maximum projection image of an ICG showing numerous CGRP-IR axons within the ganglion (40x objective lens; 1.5 μm). **B:** Single optical section image of the same ICG shown in A showing that the CGRP-IR axons move in between and surround individual ICG principal neurons. **C:** A single optical section image within the same ICG shown in A and B (2.5x zoom) showing that CGRP-IR axons formed varicosities around individual ICG principal neurons. **D:** Maximum projection image of a large CGRP-IR axon bundle within an ICG. **E-F:** Single optical

section images of the same ganglion in D at different levels. In contrast to the ganglion shown in A-C numerous CGRP-IR axons passed through this ganglion without wrapping around or forming varicosities around individual ICG principal neurons. **G-H:** Single optical section images of another ICG. Within this ICG some CGRP-IR axons wrapped around and formed varicose appositions with individual principal neurons, while others passed through the ganglion without forming appositions. *Green: CGRP-IR, Red: Autofluorescence. Scale bar: A&B, D-H: 20 μm; C: 10 μm.*
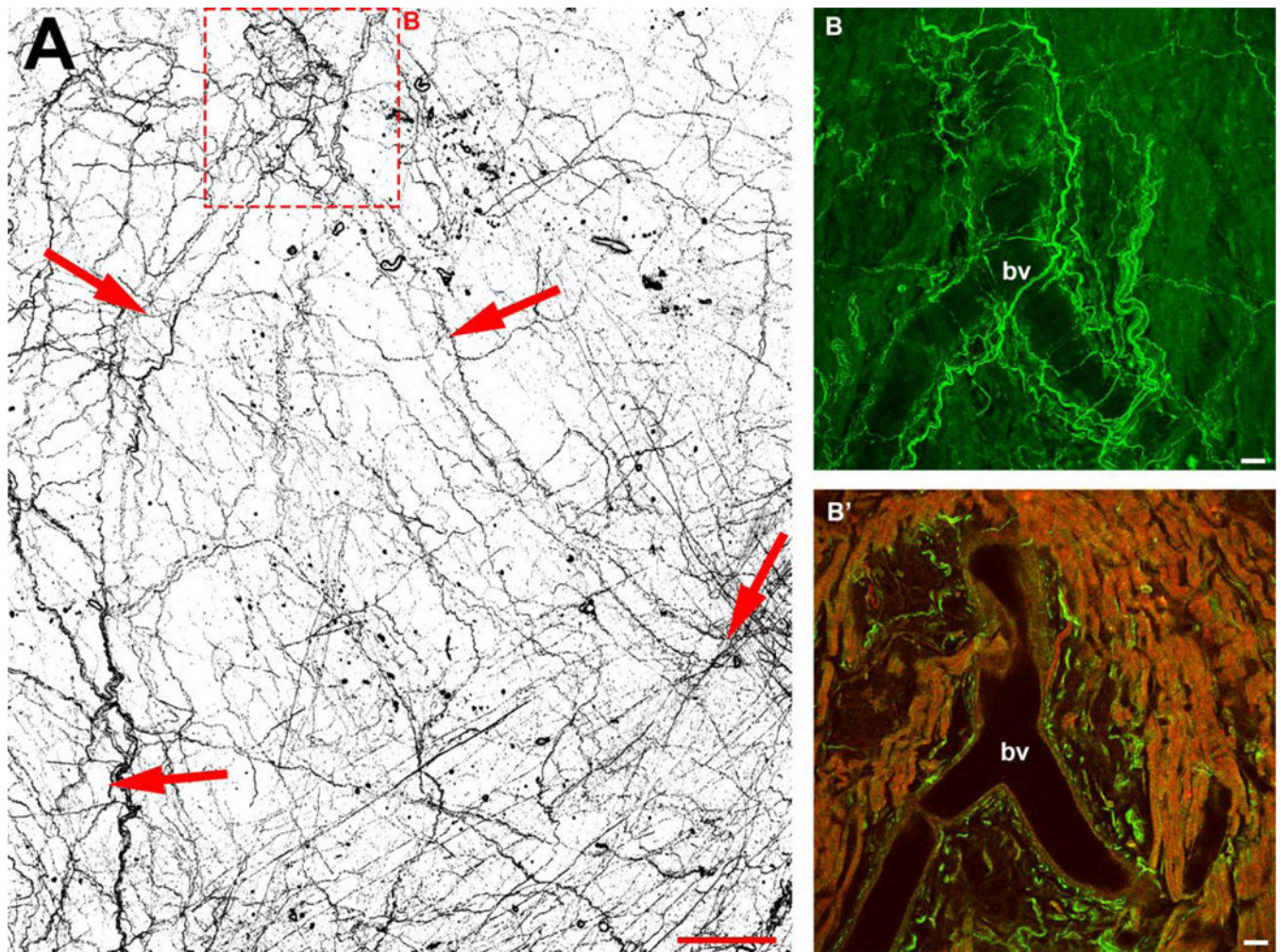
Figure 10.
CGRP-IR axons innervate blood vessels in the atria. **A:** A maximum projection montage of multiple images collected with a Zeiss M2 Imager (20x objective lens; 1.5 μm z-step) showing a small blood vessel along the surface of the IVC in the RA. **B:** Maximum projection image of a subset region of the same blood vessel in A taken with a confocal microscope (40x objective lens; 1.5 μm z-step) (20x objective lens; 1.5 μm z-step). Numerous CGRP-IR axons wrapped around the entire length of the blood vessel. **B':** Single optical section image of the subset region shown in **B** taken with a confocal microscope (40x objective lens; 1.5 μm z-step). *Green: CGRP-IR; Red: Autofluorescence; Scale bar: **A:** 200 μm; **B and B':** 20 μm.*
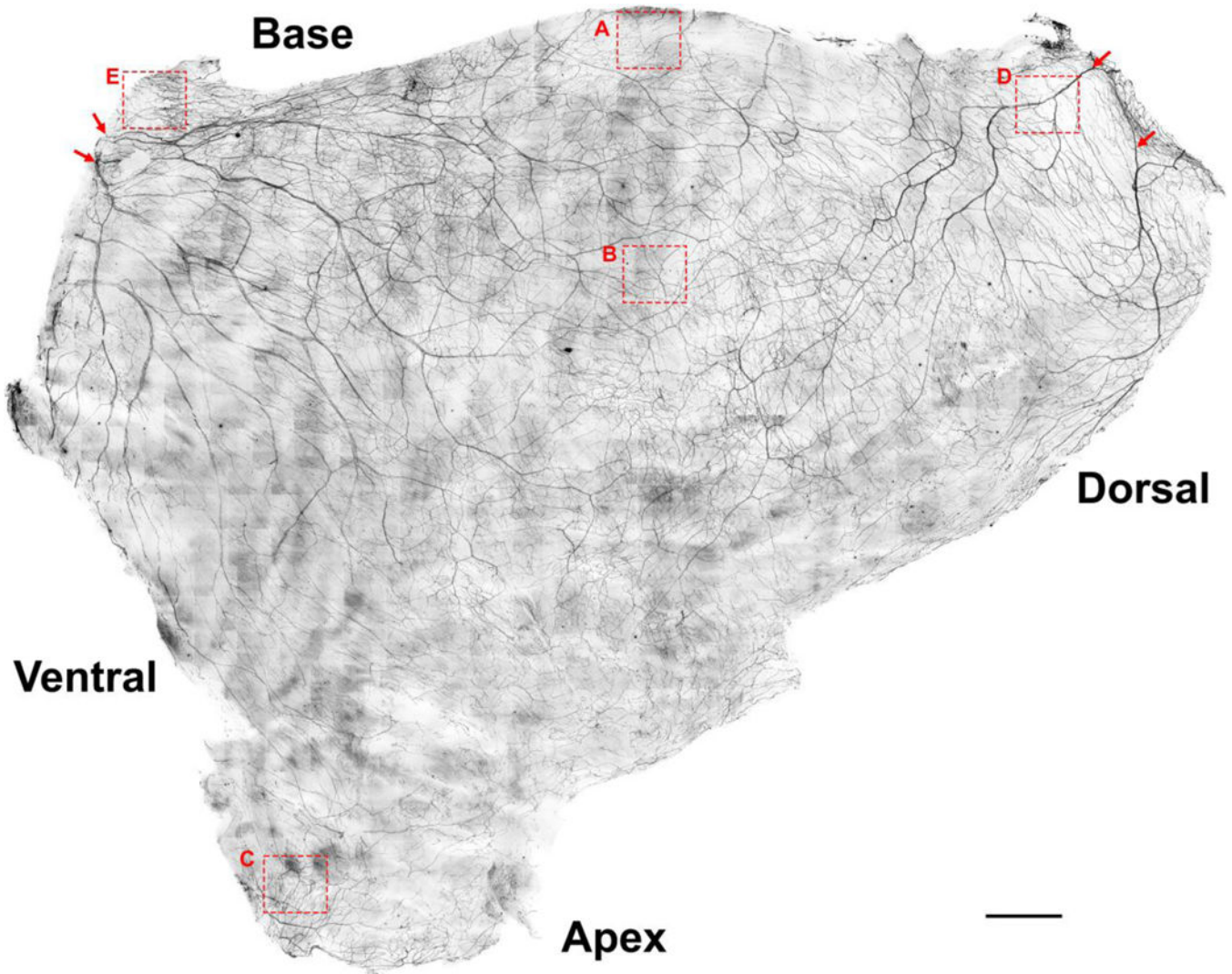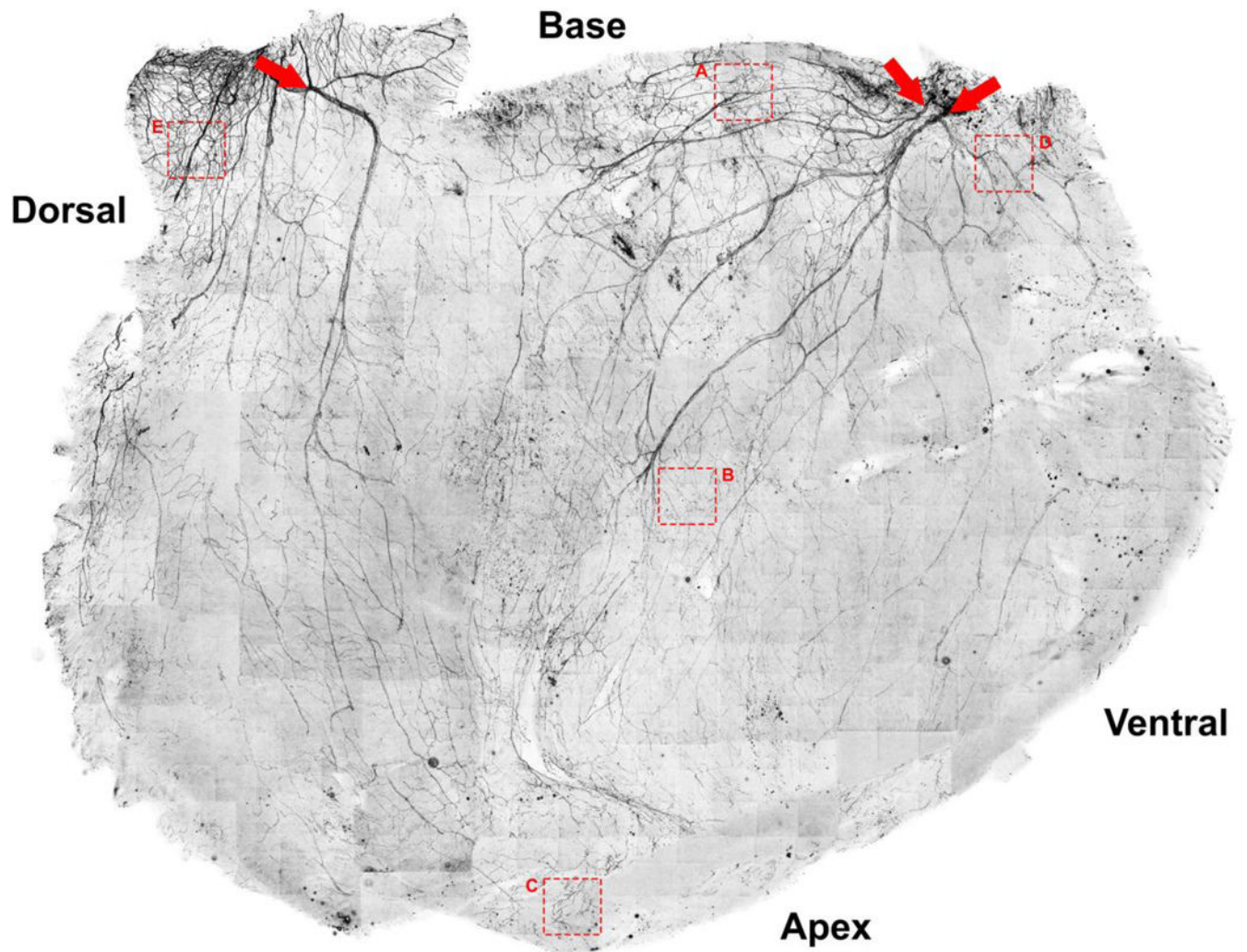
Figure 11.
Distribution of CGRP-IR axons in the right ventricle of a rat heart. CGRP-IR axons entered as large bundles along the base of the right ventricle then bifurcated into small bundles and finally formed a network of delicate fibers. Two large axon bundles entered the RV near the dorsal side of the base (adjacent to the AV node in the RA) and two large bundles entered through the ventral side of the base (arrows). In addition, many smaller axon bundles entered the RV through the middle of the base. *Scale bar: 1 mm.*
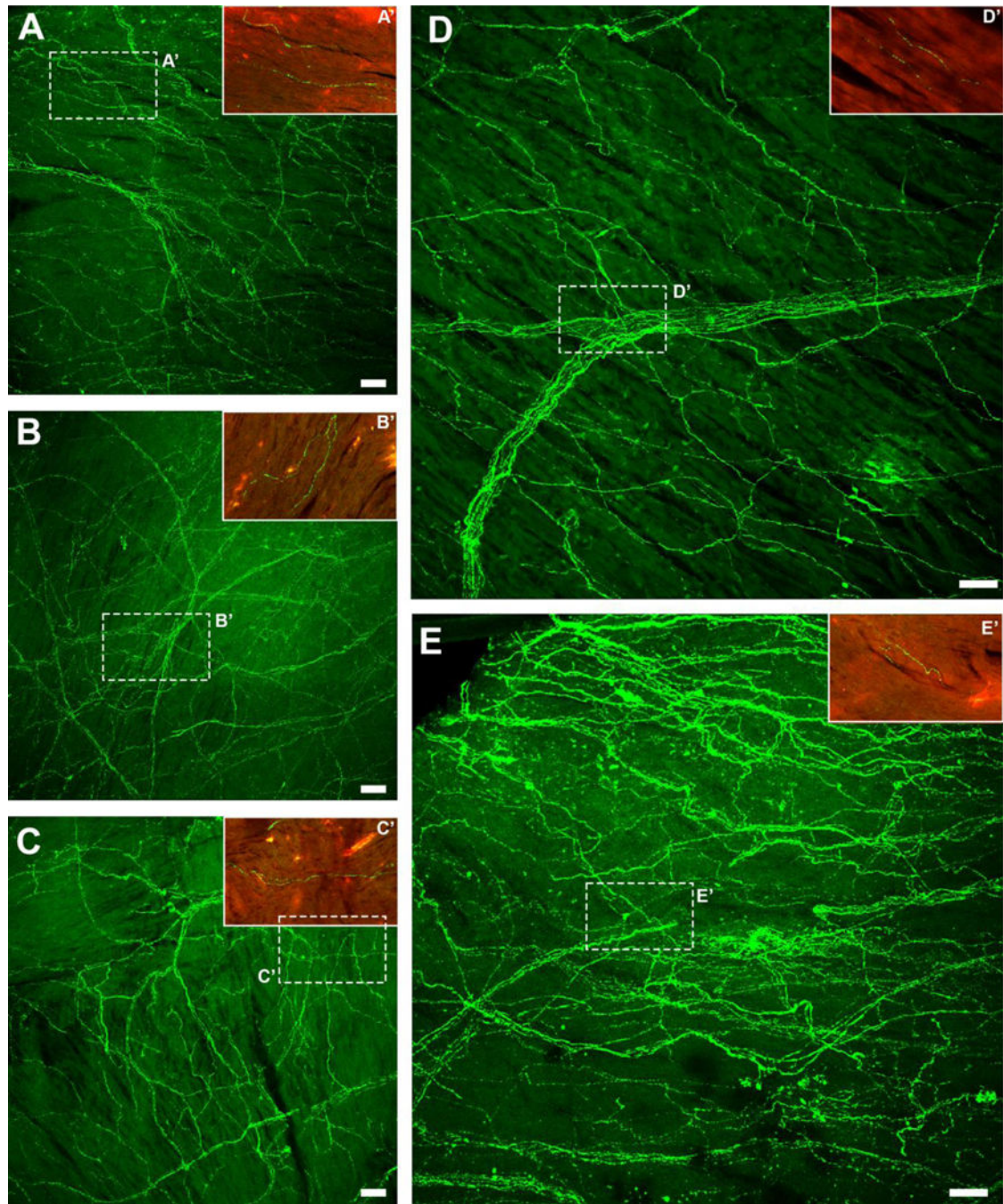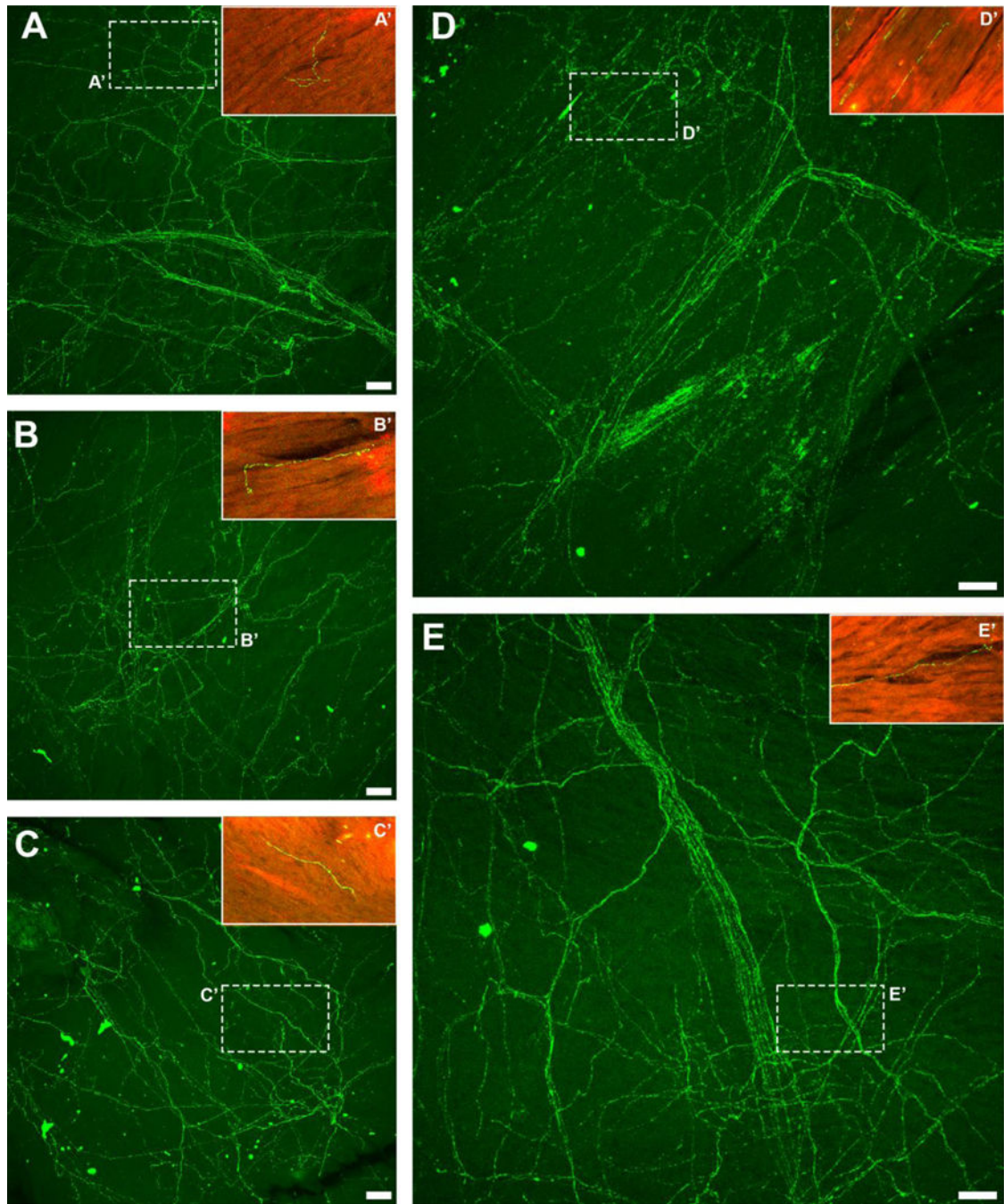
Figure 12.
CGRP-IR axons in the wall of the right ventricle (please zoom into the boxes indicated in the whole montage presented in Figure 11 to see the precise location of each of the panels in this figure). CGRP-IR axons in the muscle of the RV. **A-C:** Maximum projection images of CGRP-IR axons within the base, center, and apex of the RV, respectively. **D&E:** Maximum projection images of CGRP-IR axons within the dorsal and ventral sides of the base of the RV, respectively. **A'-E':** Single optical sections of the subset regions (white dotted boxes) in **A-E**, respectively. *Green: CGRP-IR; Red: Autofluorescence; Scale bar: 50 μm.*
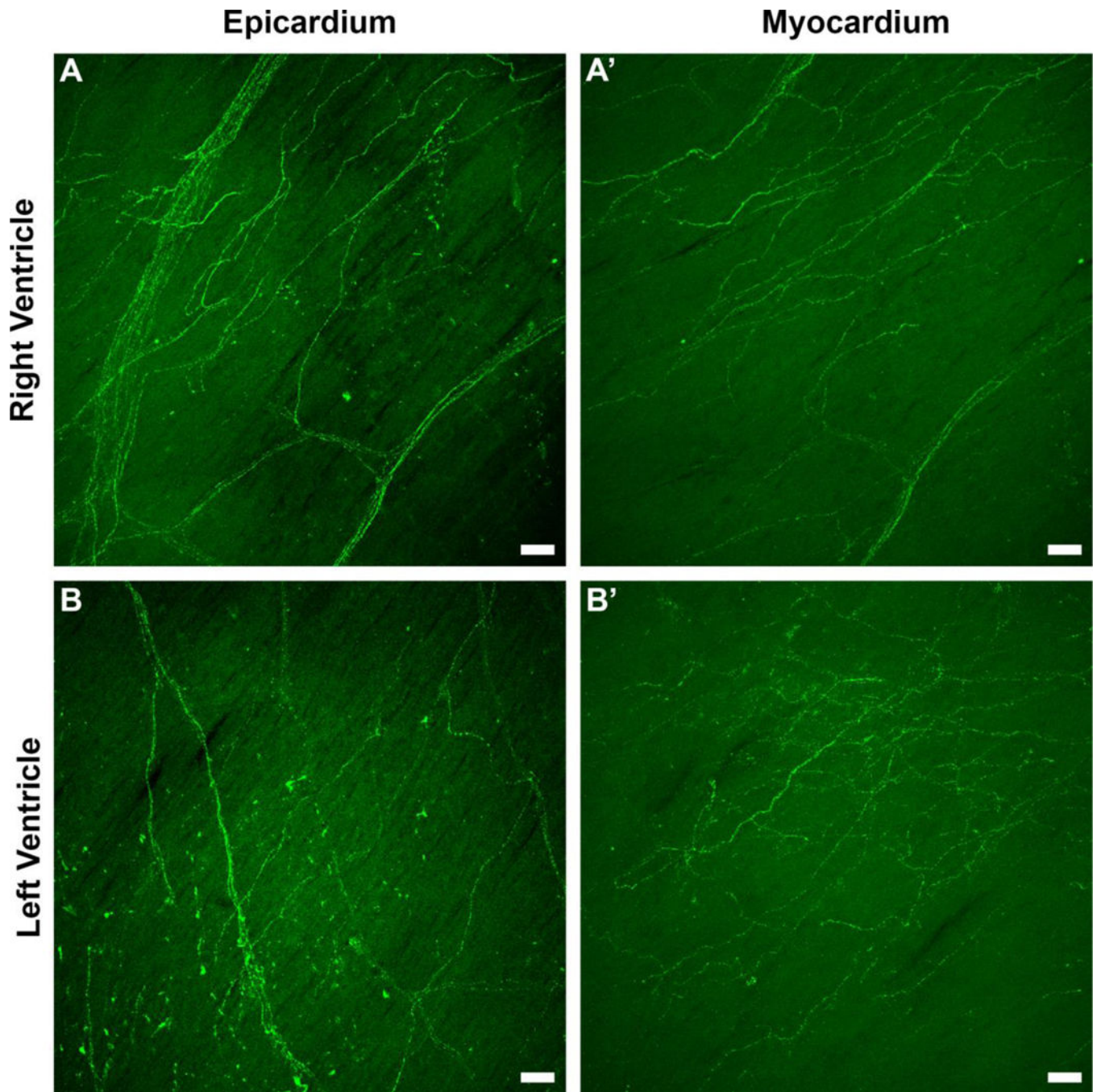
Figure 13.
Distribution of CGRP-IR fibers in the wall of the left ventricle of a rat heart. CGRP-IR axons entered as large bundles through the aorta (top left) and left pre-caval vein (LPCV, top right) (arrows) on the base of the left ventricle then bifurcated into small bundles and finally formed a network of delicate fibers. Scale bar: 1 mm.
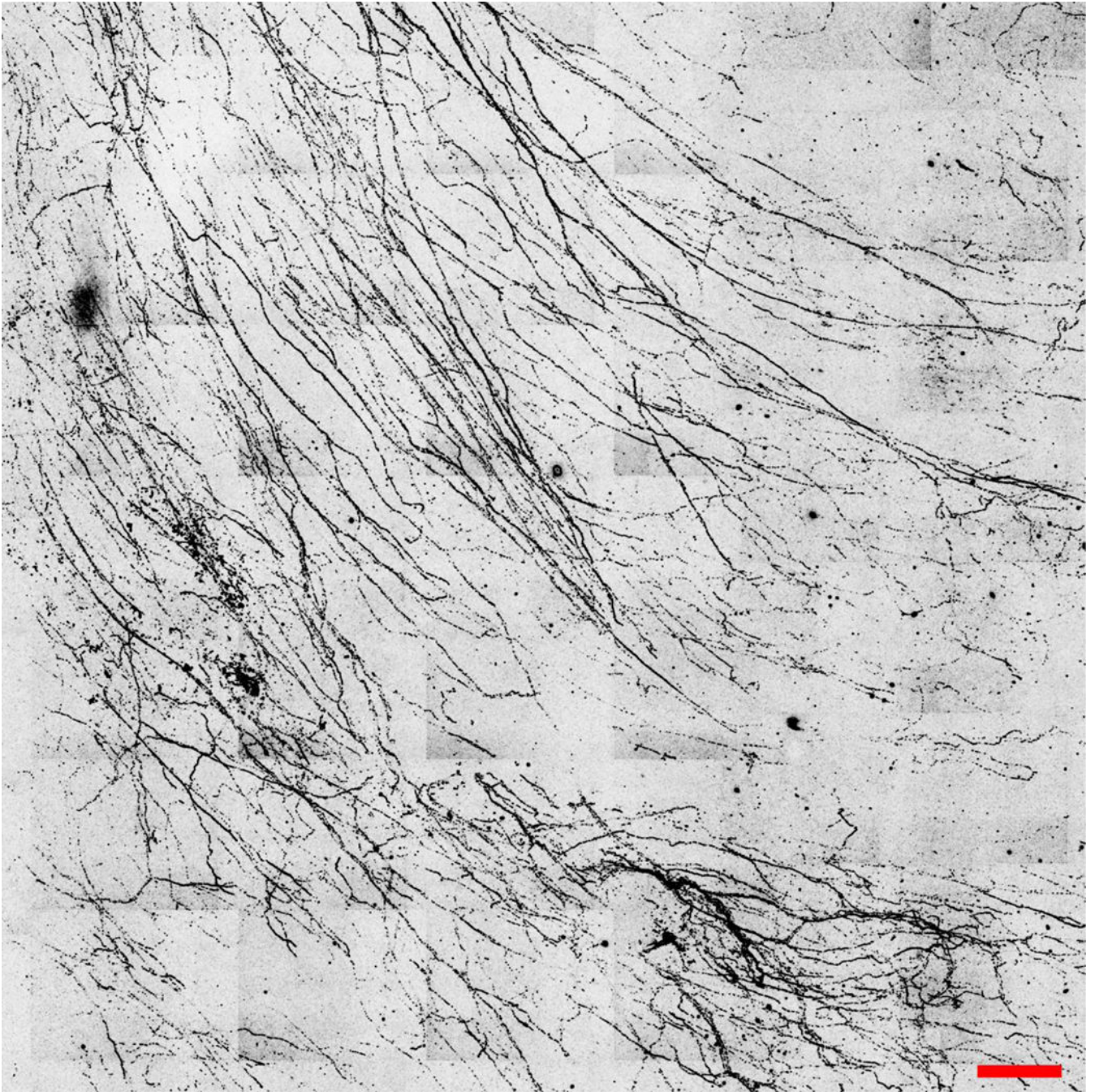
Figure 14.
CGRP-IR axons in the wall of the left ventricle (please zoom into the boxes indicated in the whole montage presented in Figure 13 to see the precise location of each of the panels in this figure). CGRP-IR axons in the muscle of the LV. **A-C:** Maximum projection images of CGRP-IR axons within the base, center, and apex of the LV, respectively. **D&E:** Maximum projection images of CGRP-IR axons within the dorsal and ventral sides of the base of the LV, respectively. **A'-E':** Single optical sections of the subset regions (white dotted boxes) in **A-E**, respectively. *Green: CGRP-IR; Red: Autofluorescence; Scale bar: 50 μm.*

Figure 15.
CGRP-IR axons in the epicardium and myocardium of the RV and LV. **A&B:** Maximum projection images CGRP-IR axons in the epicardium of the RV and LV, respectively. **A'&B':** Maximum projection images of the same locations as **A&B** showing CGRP-IR axons within the myocardium of the RV and LV, respectively. *Scale bar: 50 μm.*

Figure 16.
Distribution of CGRP-IR fibers in the interventricular septum. Stitched maximum projection images from the IVS showing a dense network of CGRP-IR axons. *Scale bar: 250 μm.*